Control Engineering Practice 85 (2019) 23–33
https://doi.org/10.1016/j.conengprac.2019.01.003
Received 20 May 2018; Received in revised form 16 October 2018; Accepted 1 January 2019
Available online xxxx
0967-0661/

Force, Orientation and Position Control in Redundant Manipulators in Prioritized Scheme with Null space Compliance.

Abbas Karami[a], Hamid Sadeghian[b,*], Mehid Keshmiri[a], Giuseppe Oriolo[c]

[a] *Mechanical Engineering Department, Isfahan University of Technology, Isfahan, Iran*
[b] *Engineering Department, University of Isfahan, Isfahan, Iran*
[c] *Dipartimento di Ingegneria Informatica, Automatica e Gestionale, Sapienza Universita di Roma, Rome, Italy*

Abstract

This paper addresses the problem of executing multiple tasks in a prioritized scheme with compliant behavior in the remaining null space for robot manipulators. In general, robot redundancy can be exploited efficiently by defining multiple tasks including safe robot interaction. When the robot experiences an accidental physical interaction in social environment during delicate manipulations, the problem of accurate and safe manipulation arises. The novel controller-observer is suggested in this work which ensures accurate accomplishment of various tasks based on a predefined hierarchy using a new priority assignment approach. Force control, position control and orientation control are considered. Moreover, a compliant behavior during accidental interaction with robot body is imposed in the null space without using joint torque measurements. Asymptotic stability of the task space error and external torque estimation error during executing multiple tasks are shown. The performance

*Corresponding author
Email addresses: a.karami@me.iut.ac.ir (Abbas Karami), h.sadeghian@eng.ui.ac.ir (Hamid Sadeghian), mehdik@cc.iut.ac.ir (Mehid Keshmiri), oriolo@diag.uniroma1.it (Giuseppe Oriolo)

of the proposed approach is evaluated on a 7R light weight robot arm in several case studies.
Keywords: Force control, Orientation control, Prioritized control, Disturbance observer, Null space compliance

1. Introduction

Robots are termed kinematically redundant when they possess more degrees of freedom (DOF) than those necessary to achieve the desired task. Redundant robots have numerous significant advantages in comparison to non-redundant ones. In addition to classical applications of redundant DOF for singularity avoidance, performance optimization, *etc.*, the possibility to define additional tasks besides the main task can also be provided. Both manipulators and humanoids robots can take this advantage to accomplish more complex tasks, effectively.

Nowadays it is essential for robots to be capable of executing various tasks in dynamic environments. Moreover, robots should ensure the safety of themselves and other entities such as a human in unknown and unpredictable places. These issues should be considered along with the accuracy of manipulation. Precise accomplishment of the tasks is critical to employ robots in delicate and vital tasks.

Task priority strategy has been developed for both first-order and second-order differential kinematics. In the prioritized control approaches, it is usual to project the Jacobian of the lower priority tasks to the null space of the higher priority tasks which ensures exact prioritization [40, 25, 10, 35, 32, 31]. These methods are known as strict prioritization approach. The alternative methods for priority assignment are non-strict approaches. Non-strict priority allocation algorithms are usually handled by employing weighting methods which a lower priority task is not enforced to execute in the null space of higher priority tasks (see for example [2] and [6]). Hence, the method does not guarantee following the desired hierarchy strictly. Recently, a method for changing gradually from

a non-strict case to a strict one is suggested in [21].

Velocity based task sequencing control with strict task priority is widely employed in different cases such as controlling the position of multiple points in [9] and visual servoing in [34, 23]. Task prioritization in acceleration level is more complex but improves the accuracy of the task execution. Prioritization method also affects the null space stability analysis. Stability analysis of the null space is critical in the acceleration level. One of the first stability analysis of the internal motion during multi-priority acceleration level control is performed by Hsu *etal*. in [11]. The stability of this algorithm has been investigated in more details in [26] and in [35]. Torque level control method is an alternative formulation which has been exploited both for humanoids [38, 19] and robotic arms [31].

Operational Space Formulation (OSF) proposed in [18] is the most common approach used for controlling the robot in the task space. Computing decoupled dynamics for the first task and designing the controller according to this dynamic constitute the basis of this formulation. In this way, handling multiple tasks is possible as it is performed in [38]. Complete stability analyses of both acceleration level and torque level approaches are performed in [36] by the authors of this paper. Recently, a new formulation with specific null space velocity coordinates has been defined in [31]. This formulation is not intuitive but the resulted coordinates which are used for compliance control of prioritized tasks simplify the stability analysis of the system.

Force control has significant applications in surgical robots [42, 7, 15, 27], industrial robots [33, 41] and humanoids [37, 19, 28]. These applications include controlling interaction force between the robot and unknown soft or hard environments. The employed methods aim to extend the application of the robots for effective execution of complex tasks. However, in all these researches force control accomplished in the absence of accidental interactions. Accidental interaction with robot body makes the control task more elaborated. In the absence of the tactile sensors which cover the robot body, observer is the most useful solution for estimating accidental interactions. Besides force control task, posi-

tion and orientation control task in other directions should be usually considered (see for example [37] and [14]). Orientation control is also a new field of interest especially in visual-servoing tasks [17]. To the best of our knowledge, force and orientation control along with position control in task space and complaint behavior in null space have not been studied so far.

In this paper, the problem of handling external interactions with robot body during executing prioritized tasks is investigated. An example of the application scenario is depicted in Fig. 1, where robot works in collaboration with a human. External interaction on the robot must be considered in the control algorithm to perform the task successfully. Previously in [36], a position control task with null space compliance is reported. In this work, a novel method for defining coordinates of the hierarchical tasks is exploited (section 3). The main purpose of this definition is to obtain an intuitive and integrated approach to prioritize multiple tasks besides introducing null space with minimal dimension. This is a critical issue to obtain the desired compliance behavior in the null space (see details in [35]).

The main contribution of this work is proposing a controller-observer algorithm to control force, position and orientation along with compliant behavior in the redundant degrees of freedom. Using external torque estimation algorithm, the execution of the prioritized tasks with minimum error is guaranteed during the accidental interaction. Asymptotic stability of the overall system is proved in section 4. The performance of the system which is evaluated experimentally on a 7DOF KUKA LWR arm is reported in Section 5.

2. Preliminaries

Herein, some critical and fundamental issues regarding this work will be reviewed. Since numerous parameters are defined and employed in this work, a nomenclature of the parameters is introduced in Table 1.

The dynamic model of an n-link robot with one physical contact point with

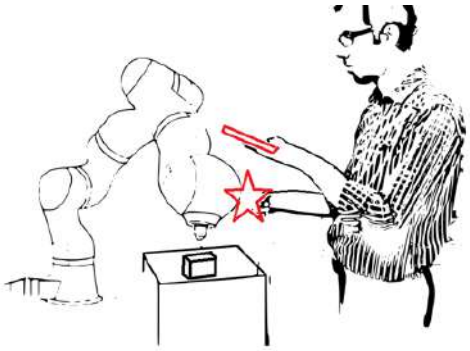

Figure 1: Accidental interaction with robot working in social environment.

the environment can be written as,

$$\boldsymbol{M}(\boldsymbol{q})\ddot{\boldsymbol{q}} + \boldsymbol{C}(\boldsymbol{q},\dot{\boldsymbol{q}})\dot{\boldsymbol{q}} + \boldsymbol{g}(\boldsymbol{q}) = \boldsymbol{\tau} - \boldsymbol{\tau}_{ext} - \boldsymbol{J}_f^T(\boldsymbol{q})\boldsymbol{f}_f, \tag{1}$$

where $\boldsymbol{M}(\boldsymbol{q}) \in \mathbb{R}^{n\times n}$ is the robot inertial matrix which depends on the robot joint configuration $\boldsymbol{q} \in \mathbb{R}^{n\times 1}$ and multiplied with joint space acceleration $\ddot{\boldsymbol{q}} \in \mathbb{R}^{n\times 1}$. $\boldsymbol{C}(\boldsymbol{q},\dot{\boldsymbol{q}})\dot{\boldsymbol{q}} \in \mathbb{R}^{n\times 1}$ represents Coriolis/centrifugal effects, gravitational torques is $(n \times 1)$ vector denoted by $\boldsymbol{g}(\boldsymbol{q})$, $\boldsymbol{\tau} \in \mathbb{R}^{n\times 1}$ is considered as the robot control torques and $\boldsymbol{\tau}_{ext} \in \mathbb{R}^{n\times 1}$ takes into account the external torques resulting from accidental interactions with the environment. Moreover, $\boldsymbol{J}_f(\boldsymbol{q}) \in \mathbb{R}^{n_f\times n}$ is Jacobian matrix of the force control task where n_f is the task dimension and $\boldsymbol{f}_f$ is $(n_f \times 1)$ intentional contact force vector applied to the robot. In the case of multi-contact problem $\boldsymbol{J}_f^T(\boldsymbol{q})\boldsymbol{f}_f$ should be replaced with proper term including all the contact forces.

Considering r different tasks, the i-th task coordinate vector $\boldsymbol{x}_i \in \mathbb{R}^{n_i}$ is related to the joint space vector through the mapping $\boldsymbol{x}_i = \boldsymbol{h}_i(\boldsymbol{q})$ for $1 \leq i \leq r$. Hence, the task space velocities $\dot{\boldsymbol{x}}_i$ are related to the joint space velocities $\dot{\boldsymbol{q}}$ by

$$\dot{\boldsymbol{x}}_i = \boldsymbol{J}_i(\boldsymbol{q})\dot{\boldsymbol{q}}, \tag{2}$$

where $\boldsymbol{J}_i(\boldsymbol{q}) = \frac{\partial \boldsymbol{h}_i}{\partial \boldsymbol{q}}$ is the Jacobian matrix of the i-th task. In the case of position control tasks, following the operational space formulation introduced

Table 1: Nomenclature

Variable	Description
$\boldsymbol{q}$	Robot joint configuration vector
t	Time
$\boldsymbol{M}(\boldsymbol{q})$	Robot inertial matrix in joint space
$\boldsymbol{C}(\boldsymbol{q}, \dot{\boldsymbol{q}})$	Robot coriolis/centrifugal matrix in joint space
$\boldsymbol{g}(\boldsymbol{q})$	Robot gravity vector in joint space
$\boldsymbol{\tau}$	Robot control torque in joint space
$\boldsymbol{J}(\boldsymbol{q})$	Robot jacobian matrix
$\boldsymbol{J}_i(\boldsymbol{q})$	i-th task jacobian matrix
$\boldsymbol{J}_f(\boldsymbol{q})$	Physical contact jacobian matrix
$\bar{\boldsymbol{J}}_i(\boldsymbol{q})$	New jacobian of the i-th task
$\boldsymbol{J}_{aug,i}(\boldsymbol{q})$	Augmentation of the new jacobian matrices from 1 to i
$\boldsymbol{\tau}_{ext}$	External accidental torque
$\boldsymbol{\Lambda}_i(\boldsymbol{q})$	Inertial matrix in the i-th task space
$\boldsymbol{\mu}_i(\boldsymbol{q}, \dot{\boldsymbol{q}})$	Coriolis/centrifugal vector in the i-th task space
$\boldsymbol{p}_i(\boldsymbol{q})$	Gravity vector in the i-th task space
$\boldsymbol{f}_{control,i}$	Control command in i-th task space
$\boldsymbol{f}_f$	Intentional contact force
$\boldsymbol{Z}_i(\boldsymbol{q})$	Null space based matrix for the i-th task
$\boldsymbol{P}_i(\boldsymbol{q})$	Null space projector of for i-th task
$\boldsymbol{x}$	Operational space coordinates for the i-th task
$\bar{\boldsymbol{x}}$	New operational space coordination for the i-th task
$\boldsymbol{\nu}$	Null space velocity coordinates
$\boldsymbol{p}(t)$	Linear momentum
$\boldsymbol{r}(t)$	Residual vector
$\boldsymbol{K}_{env}$	Environment stiffness
$\boldsymbol{C}_{env}$	Environment damping
$\boldsymbol{K}_{obs}$	Observer gain

$\boldsymbol{K}_{i,d}$	Derivative gain for the i-th operational space Error
$\boldsymbol{K}_{i,p}$	Proportional gain for the i-th operational space Error
$\boldsymbol{K}_{i,i}$	Integral gain for the the i-th operational space Error
$\boldsymbol{R}_e$	Rotation matrix of the end effector
$\boldsymbol{\omega}_k^j$	Angular velocity of link "k" w.r.t frame "j"
$\boldsymbol{\eta}_k$	Scaler part of quaternion representation of the orientation of "k"
$\boldsymbol{\varepsilon}_k^j$	Vector part of quaternion representation of the orientation of link "k" w.r.t frame "j"

in [18], the i-th task space dynamics can be written as

$$\boldsymbol{\Lambda}_i(\boldsymbol{q})\ddot{\boldsymbol{x}}_i + \boldsymbol{\mu}_i + \boldsymbol{p}_i(\boldsymbol{q}) = \boldsymbol{f}_{control,i} - \boldsymbol{f}_f - \boldsymbol{J}_i^{\#^T}(\boldsymbol{q})\boldsymbol{\tau}_{ext}, \tag{3}$$

where

$$\begin{aligned} \boldsymbol{\Lambda}_i(\boldsymbol{q}) &= (\boldsymbol{J}_i(\boldsymbol{q})\boldsymbol{M}^{-1}(\boldsymbol{q})\boldsymbol{J}_i^T(\boldsymbol{q}))^{-1}, \\ \boldsymbol{\mu}_i(\boldsymbol{q},\dot{\boldsymbol{q}}) &= \boldsymbol{J}_i^{\#^T}(\boldsymbol{q})\boldsymbol{C}(\boldsymbol{q},\dot{\boldsymbol{q}})\dot{\boldsymbol{q}} - \boldsymbol{\Lambda}_i(\boldsymbol{q})\dot{\boldsymbol{J}}_i(\boldsymbol{q})\dot{\boldsymbol{q}}, \\ \boldsymbol{p}_i(\boldsymbol{q}) &= \boldsymbol{J}_i^{\#^T}(\boldsymbol{q})\boldsymbol{g}(\boldsymbol{q}). \end{aligned} \tag{4}$$

$\boldsymbol{\Lambda}_i(\boldsymbol{q}) \in \mathbb{R}^{n_i \times n_i}$, $\boldsymbol{\mu}_i(\boldsymbol{q}) \in \mathbb{R}^{n_i \times n_i}$ and $\boldsymbol{p}_i(\boldsymbol{q}) \in \mathbb{R}^{n_i \times 1}$ are the inertial matrix, Coriolis/centrifugal vector and gravity vector in i-th task space, respectively. $\boldsymbol{f}_{control,i}$ is a $(n_i \times 1)$ vector represents the i-th task control command and $\boldsymbol{J}_i^{\#}(\boldsymbol{q}) \in \mathbb{R}^{n \times n_i}$ denotes the inertial weighted generalized inverse of the i-th task Jacobian [18]. Control torque is related to task control command through $\boldsymbol{\tau} = \Sigma_{i=1}^{i=r}\boldsymbol{J}_i{}^T(\boldsymbol{q})\boldsymbol{f}_{control,i}$. Using proper projected Jacobian along with their dynamically consistent generalized inverse insures decoupled inertial matrix [20, 32] as [1]

$$\boldsymbol{\Lambda} = diag(\boldsymbol{\Lambda}_1, \boldsymbol{\Lambda}_2, \dots \boldsymbol{\Lambda}_r). \tag{5}$$

We are looking for a task prioritization scheme with the following specifications,

- Lower priority tasks do not disturb the higher ones. In other words, the j-th task should not disturb the i-th task where $j > i \geq 1$.

[1] Variable dependencies in $\boldsymbol{q}$ and $\dot{\boldsymbol{q}}$ are shown in the in the first usage of variables and omitted elsewhere for the sake of clarity

- The dimension of the lowest level of hierarchy should be obtained as $n_r = n - \sum_{i=1}^{r-1} n_i$, which means that, we introduce the null space dynamics with n_r independent coordinates.

3. Problem Formulation

In order to obtain a prioritized scheme with aforementioned characteristics, a new set of coordinates is needed. Hence, $\bar{\boldsymbol{J}}_i(\boldsymbol{q})$ is the $(n_i \times n)$ matrix proposed as

$$\bar{\boldsymbol{J}}_i(\boldsymbol{q}) = \begin{cases} \boldsymbol{J}_1 & i = 1 \\ \boldsymbol{J}_i \boldsymbol{Z}_{i-1}^T (\boldsymbol{Z}_{i-1} \boldsymbol{M} \boldsymbol{Z}_{i-1}^T)^{-1} \boldsymbol{Z}_{i-1} \boldsymbol{M} & i = 2, ..., r-1 \\ (\boldsymbol{Z}_{r-1} \boldsymbol{M} \boldsymbol{Z}_{r-1}^T)^{-1} \boldsymbol{Z}_{r-1} \boldsymbol{M} & i = r, \end{cases} \tag{6}$$

where $\boldsymbol{Z}_{i-1}(\boldsymbol{q}) \in \mathbb{R}^{n - \sum_{j=1}^{i-1} n_j \times n}$ spans the complete null space of all previous tasks with minimal necessary dimension. Constructing $\boldsymbol{Z}_{i-1}$ is not unique and special care must be taken for its computation. Singular value decomposition can be utilized to obtain null space base Jacobian $\boldsymbol{Z}_{i-1}$. However, we have used analytical method discussed in [30] to ensure matrix continuity. For this purpose, the augmented Jacobian matrix is constructed as,

$$\boldsymbol{J}_{aug,i} = \begin{bmatrix} \bar{\boldsymbol{J}}_1 \\ \bar{\boldsymbol{J}}_2 \\ \vdots \\ \bar{\boldsymbol{J}}_i \end{bmatrix}. \tag{7}$$

and null space base matrices for computation of the Jacobian of the tasks $2, ..., i$ are obtained such that

$$\boldsymbol{J}_{aug,i} \boldsymbol{Z}_i^T = \boldsymbol{0}. \tag{8}$$

In (6), $\boldsymbol{Z}_{i-1}^T (\boldsymbol{Z}_{i-1} \boldsymbol{M} \boldsymbol{Z}_{i-1}^T)^{-1} \boldsymbol{Z}_{i-1} \boldsymbol{M}$ is the projection operator to the space where the rows of $\boldsymbol{Z}_{i-1}$ are its base vectors. Similar operator definition can be found for example in [30], but to the best of our knowledge, it has not been employed for prioritization multiple tasks till now. Calling this projector as

$\boldsymbol{T}_{i-1} \in \mathbb{R}^{n\times n}$, it is obvious that $\boldsymbol{T}_{i-1}$ is idempotent and also fulfills $\boldsymbol{T}_{i-1}\boldsymbol{Z}_{i-1}^T = \boldsymbol{Z}_{i-1}^T$. $\bar{\boldsymbol{J}}_r$ dimension is $(n - \sum_{i=1}^{r-1} n_i \times n)$ which is a significant feature to obtain the desired stable behavior in the null space of the higher priority tasks (for more details [26] and [35] are referred).

The kinematic relation between the joint and task space velocities are then given as

$$\dot{\tilde{\boldsymbol{x}}} = \boldsymbol{J}_{aug,r}\dot{\boldsymbol{q}}. \tag{9}$$

Denoting that by using (6), $\boldsymbol{J}_{aug,r}$ is $(n \times n)$ nonsingular matrix for full rank and independent $\boldsymbol{J}_i$. $\dot{\tilde{\boldsymbol{x}}}$ and $\dot{\boldsymbol{q}}$ are $(n \times 1)$ task and joint space velocity vectors. For given task velocity, the general solution for (9) can be written as

$$\dot{\boldsymbol{q}} = \boldsymbol{J}_{aug,r}^{-1}\dot{\tilde{\boldsymbol{x}}}, \tag{10}$$

where $\dot{\tilde{\boldsymbol{x}}} = [\dot{\tilde{\boldsymbol{x}}}_1, \dot{\tilde{\boldsymbol{x}}}_2, \ldots, \dot{\tilde{\boldsymbol{x}}}_{r-1}, \boldsymbol{\nu}]^T$. $\boldsymbol{\nu}$ is $(n_r \times 1)$ null space velocity vector which is in general non-integrable [22].

Dynamically consistent generalized inverse $\bar{\boldsymbol{J}}_i^{\#}$ is defined as

$$\bar{\boldsymbol{J}}_i^{\#} = \begin{cases} \boldsymbol{M}^{-1}\bar{\boldsymbol{J}}_i{}^T(\bar{\boldsymbol{J}}_i\boldsymbol{M}^{-1}\bar{\boldsymbol{J}}_i{}^T)^{-1} & i = 1, ..., r-1, \\ \boldsymbol{Z}_{r-1}^T & i = r. \end{cases} \tag{11}$$

and by exploiting (7) and (8) along with (6) we have

$$\begin{cases} \boldsymbol{J}_1\boldsymbol{Z}_1^T = 0, & i = 1, \\ \boldsymbol{J}_j\boldsymbol{Z}_{j-1}^T(\boldsymbol{Z}_{j-1}\boldsymbol{M}\boldsymbol{Z}_{j-1}^T)^{-1}\boldsymbol{Z}_{j-1}\boldsymbol{M}\boldsymbol{Z}_i^T = 0, & i = 2, ..., r, \end{cases} \tag{12}$$

for $j \leq i$. Recent relations can be exploited to ensure the fulfillment of

$$\boldsymbol{J}_{aug,i-1}\bar{\boldsymbol{J}}_i^{\#} = \boldsymbol{0}, \tag{13}$$

and

$$\bar{\boldsymbol{J}}_j\boldsymbol{M}^{-1}\bar{\boldsymbol{J}}_i^T = \boldsymbol{0} \qquad \text{for any } i \text{ and } j. \tag{14}$$

Equation (13) guarantees the order of priority as shown in Fig. 2. Restriction of the lower priority tasks when they conflict with the higher priority tasks is demonstrated by using solid and dashed lines in Fig. 2. Moreover (14) ensures

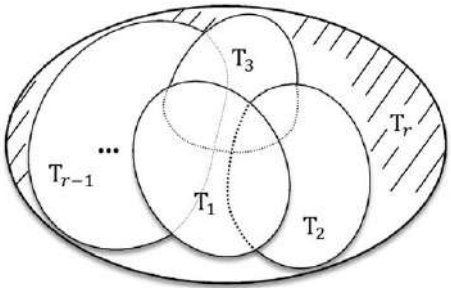

Figure 2: Graphical interpretation of hypothetical prioritized tasks in the joint space. T_i shows the i-th task and T_r (shaded) is the null space of all major tasks. While solid lines display the boundary of each task which is accessible in hierarchical scheme, dashed lines describe the omitted part of the task with respect to the priority allocation.

dynamical consistency and block diagonal inertia matrix [31]. By observing (14), one can show

$$\boldsymbol{J}_{aug,r}^{-1} = \left[\begin{array}{cccc} \bar{\boldsymbol{J}}_1^{\#} & \bar{\boldsymbol{J}}_2^{\#} & \dots & \bar{\boldsymbol{J}}_r^{\#} \end{array} \right], \tag{15}$$

employing similar approach followed in [29] and [35].

Equation (10) can be extended to the second order kinematic solution as

$$\ddot{\boldsymbol{q}} = \boldsymbol{J}_{aug,r}^{-1}(\ddot{\tilde{\boldsymbol{x}}} - \dot{\boldsymbol{J}}_{aug,r}\dot{\boldsymbol{q}}), \tag{16}$$

where

$$\ddot{\tilde{\boldsymbol{x}}} = \begin{bmatrix} \ddot{\bar{\boldsymbol{x}}}_1 \\ \ddot{\bar{\boldsymbol{x}}}_2 \\ \vdots \\ \ddot{\bar{\boldsymbol{x}}}_{r-1} \\ \dot{\boldsymbol{\nu}} \end{bmatrix}. \tag{17}$$

Consequently, using (6) and (11) the i-th level decoupled dynamic is realized as

$$\bar{\boldsymbol{\Lambda}}_i(\boldsymbol{q})\ddot{\bar{\boldsymbol{x}}}_i + \bar{\boldsymbol{\mu}}_i(\boldsymbol{q}, \dot{\boldsymbol{q}}) + \bar{\boldsymbol{p}}_i(\boldsymbol{q}) = \bar{\boldsymbol{f}}_{control,i} - \bar{\boldsymbol{J}}_i^{\#^T}(\boldsymbol{q})\boldsymbol{\tau}_{ext}, \tag{18}$$

where $\bar{\boldsymbol{\Lambda}}_i(\boldsymbol{q})$, $\bar{\boldsymbol{\mu}}_i(\boldsymbol{q})$ and $\bar{\boldsymbol{p}}_i(\boldsymbol{q})$ are computed by replacing $\boldsymbol{J}_i$ and $\boldsymbol{J}_i^{\#}$ with $\bar{\boldsymbol{J}}_i$ and $\bar{\boldsymbol{J}}_i^{\#}$ in (4) and (3) and $\boldsymbol{\tau} = \Sigma_{i=1}^{i=n} \bar{\boldsymbol{J}}_i{}^T(\boldsymbol{q})\bar{\boldsymbol{f}}_{control,i}$. It is noteworthy that for

the force control task, $-\boldsymbol{f}_f$ which is the force vector applied to the force control task space should be added to the right side of (18).

Thanks to the Jacobian definition in (6), $n_r = n - \sum_{i=1}^{r-1} n_i$ and r decoupled task space dynamics (similar to (18)) can be obtained which facilitate the control of several tasks simultaneously. Moreover, null space dynamics is clear and it is possible to handle the physical interactions besides accomplishing the tasks. In other words, a compliance behavior can be obtained during physical interaction in the null space. It is noteworthy that according to the comparison between different methods for defining orientation error reported in [4], the unit quaternion formulation is employed for orientation tasks in the present work.

Denoting the command acceleration in the i-th task space with $\ddot{\boldsymbol{x}}_{c,i}$ and in the null space by $\dot{\boldsymbol{\nu}}_c$, manipulator control torque can be computed through

$$\begin{aligned}\boldsymbol{\tau} =& \sum_{i=1}^{r-1} \bar{\boldsymbol{J}}_i^T (\bar{\boldsymbol{\Lambda}}_i (\ddot{\boldsymbol{x}}_{c,i} - \dot{\bar{\boldsymbol{J}}}_i \dot{\boldsymbol{q}})) + \bar{\boldsymbol{J}}_r^T (\bar{\boldsymbol{\Lambda}}_r (\dot{\boldsymbol{\nu}}_c - \dot{\bar{\boldsymbol{J}}}_r \dot{\boldsymbol{q}})) \\ &+ \boldsymbol{J}_f^T \boldsymbol{f}_f + \boldsymbol{C}\dot{\boldsymbol{q}} + \boldsymbol{g}.\end{aligned} \tag{19}$$

Considering (11), (18) and (19), one can simplifies the task space closed-loop dynamics as

$$\bar{\boldsymbol{\Lambda}}_i [\ddot{\boldsymbol{x}} - \ddot{\boldsymbol{x}}_c + \bar{\boldsymbol{J}}_i M^{-1} \boldsymbol{\tau}_{ext}] = \boldsymbol{0}, \tag{20}$$

which clearly shows the significant effect of the external physical interaction torque on the robot performance. According to the paper intention, the major issues in the following section are:

- Proposing controller-observer for accurate, efficient and safe force, position and orientation control along with compliance in the null space.
- Discussing the stability of the manipulator by employing the new force, position and orientation control commands besides the method proposed in [35] for position control in any arbitrary task combination.

4. Controller Design and Stability

In this section, we propose a new controller-observer algorithm based on *generalized momentum observer*. In our previous work [36], the generalized momentum observer, originally proposed in [8], has been exploited effectively to control the interaction during task space control. In that work, we mainly considered the regulation of the task space position around a desired position. Here a novel method for controlling force and orientation tasks is proposed. Meanwhile the stability analysis covers multiple force, orientation and position control or any combination of them besides compliance in the null space. The Jacobian definition in equation (6) and the analysis in the previous section enable us to achieve this goal properly.

4.1. Controller Design

By using the dynamics equation (1), n-dimensional residual vector $\boldsymbol{r}$ is defined as

$$\boldsymbol{r}(t) = \boldsymbol{K}_{obs}[\boldsymbol{p}(t) - \int_0^t (\boldsymbol{\tau} + \boldsymbol{C}^T\dot{\boldsymbol{q}} - \boldsymbol{g} - \boldsymbol{J}_f^T\boldsymbol{f}_f + \boldsymbol{r}(\sigma))d\sigma], \tag{21}$$

where $\boldsymbol{p}(t) = \boldsymbol{M}\dot{\boldsymbol{q}}$, $\boldsymbol{p}(0) = \boldsymbol{0}$, $\boldsymbol{r}(0) = \boldsymbol{0}$ and $\boldsymbol{K}_{obs} \in \mathbb{R}^{n\times n}$ is a positive definite matrix. It can be shown that the residual vector dynamics is

$$\dot{\boldsymbol{r}} = -\boldsymbol{K}_{obs}r - \boldsymbol{K}_{obs}\boldsymbol{\tau}_{ext}. \tag{22}$$

Hence, by choosing proper $\boldsymbol{K}_{obs}$, accidental physical interactions with robot body can be estimated through (21). It is noteworthy that intentional interaction with robot body for force control task ($\boldsymbol{f}_f$) is not included in the realized estimation.

Observing (20), it is obvious that any accidental contact with the robot body may produce deviation from the assigned task. Proper command acceleration can handle undesired motions and reduce the task errors. For accurate task execution, the command accelerations for force, position and orientation control are proposed as

$$\ddot{\boldsymbol{x}}_{cf} = \boldsymbol{K}_{f,p}\tilde{\boldsymbol{f}} + \boldsymbol{K}_{f,i}\int \tilde{\boldsymbol{f}}d\sigma - \boldsymbol{K}_{f,d}\dot{\tilde{\boldsymbol{x}}}_f - \bar{\boldsymbol{\Lambda}}_f^{-1}\bar{\boldsymbol{J}}_f^{\#^T}\boldsymbol{r}, \tag{23}$$

$$\ddot{\boldsymbol{x}}_{cp} = -\boldsymbol{K}_{p,d}\dot{\tilde{\boldsymbol{x}}} + \boldsymbol{K}_{p,p}\tilde{\boldsymbol{x}} - \bar{\boldsymbol{\Lambda}}_p^{-1}\bar{\boldsymbol{J}}_p^{\#^T}\boldsymbol{r}, \tag{24}$$

$$\ddot{\boldsymbol{x}}_{co} = -\boldsymbol{K}_{o,d}\bar{\boldsymbol{\omega}}_e + \boldsymbol{K}_{o,p}\boldsymbol{\varepsilon}_{de} - \bar{\boldsymbol{\Lambda}}_o^{-1}\bar{\boldsymbol{J}}_o^{\#^T}\boldsymbol{r}. \tag{25}$$

Here, $\tilde{\boldsymbol{f}} = \boldsymbol{f}_d - \boldsymbol{f}_f$ is the force control error and $\dot{\tilde{\boldsymbol{x}}}_f$ is the velocity vector in the force control direction. $\boldsymbol{K}_{f,i} \in \mathbb{R}^{n_f \times n_f}$, $\boldsymbol{K}_{f,p} \in \mathbb{R}^{n_f \times n_f}$ and $\boldsymbol{K}_{f,d} \in \mathbb{R}^{n_f \times n_f}$ are positive definite gains in the force control space. For position control tasks, $\boldsymbol{x}$ is the task space variable and $\tilde{\boldsymbol{x}} = \boldsymbol{x}_d - \boldsymbol{x}$. In (25), $\bar{\boldsymbol{\omega}}_e$ and $\boldsymbol{\varepsilon}_{de}$ are the end effector angular velocity vector and the vector part of the quaternion parameters extracted from mutual rotation matrix $\boldsymbol{R}_d^e$ in the base frame. $\boldsymbol{K}_{p,p} \in \mathbb{R}^{n_p \times n_p}$, $\boldsymbol{K}_{p,d} \in \mathbb{R}^{n_p \times n_p}$, $\boldsymbol{K}_{o,p} \in \mathbb{R}^{n_o \times n_o}$ and $\boldsymbol{K}_{o,d} \in \mathbb{R}^{n_o \times n_o}$ are positive definite matrices considered as position and orientation control gains when n_p and n_o are corresponding task space dimensions.

Thanks to the robot redundancy, compliant behavior can be imposed in the null space of major tasks with the null space command acceleration

$$\dot{\boldsymbol{\nu}}_c = -\bar{\boldsymbol{\Lambda}}_r^{-1}((\bar{\boldsymbol{\mu}}_r + \boldsymbol{B}_r)\boldsymbol{\nu} - \boldsymbol{Z}_{r-1}\boldsymbol{K}_{r,p}\tilde{\boldsymbol{q}}) \tag{26}$$

where $\tilde{\boldsymbol{q}} = \boldsymbol{q}_d - \boldsymbol{q}$ with $\boldsymbol{q}_d \in \mathbb{R}^{n \times 1}$ as a desired joint space configuration and $\boldsymbol{B}_r \in \mathbb{R}^{n_r \times n_r}$ is a positive definite matrix. These command accelerations are further used in (19) to construct manipulator control torque.

Proposition 1: Assume that the external torque ($\boldsymbol{\tau}_{ext}$) is constant (or slowly time varying). The control command (19) besides the command accelerations (23)-(26) and the residual vector (21) guarantee that the task space and torque estimation errors go to zero asymptotically. Moreover, a desired compliant behavior is imposed in the null space of the main tasks.

4.2. Stability Analysis

In this section stability analysis of the proposed controller-observer is performed. First, some preliminary theorems and lemmas are given. Afterward, in

subsection 4.2.2 the above proposition is clarified and proved. In the proof, independent main tasks are considered and dependent tasks are discussed separately at the end of that subsection.

4.2.1. Preliminary Theorems

Theorem 2 [12]: Consider the system $\dot{\boldsymbol{z}} = h(\boldsymbol{z})$ with $\boldsymbol{z} = 0$ as equilibrium point. If a function $V(\boldsymbol{z}) \in C^1(\Omega, \mathbb{R})$ on the neighborhood Ω of the origin exists such that

- $V(\boldsymbol{z}) \geq 0$ for all $\boldsymbol{z} \in \Omega$ and $V(0) = 0$;
- $\dot{V}(\boldsymbol{z}) \leq 0$ for all $\boldsymbol{z} \in \Omega$;
- The system is asymptotically stable in the largest positively invariant set $\mathcal{L}$ contained in $\{\boldsymbol{z} \in \Omega | \dot{V}(\boldsymbol{z}) = 0\}$;

the origin is then asymptotically stable.

Lemma 3 [16]: Consider the dynamical system $\dot{\boldsymbol{z}} = f(\boldsymbol{z}, t) + d(\boldsymbol{z}, t)$ where $f(\boldsymbol{z}, t)$ is the nominal system and $d(\boldsymbol{z}, t)$ is the perturbation term. Let $\boldsymbol{z} = 0$ be an exponentially stable equilibrium point for the nominal system ($\dot{\boldsymbol{z}} = f(\boldsymbol{z}, t)$) and $V(\boldsymbol{z}, t)$ be a Lyapunov function for the nominal system such that

$$C_1 \parallel \boldsymbol{z} \parallel^2 \leq V(\boldsymbol{z}, t) \leq C_2 \parallel \boldsymbol{z} \parallel^2, \tag{27}$$

$$\frac{\partial V}{\partial t} + \frac{\partial V}{\partial \boldsymbol{z}} f(\boldsymbol{z}) \leq -C_3 \parallel \boldsymbol{z} \parallel^2, \tag{28}$$

$$\parallel \frac{\partial V}{\partial \boldsymbol{z}} \parallel \leq C_4 \parallel \boldsymbol{z} \parallel, \tag{29}$$

and the perturbation term $d(\boldsymbol{z}, t)$ satisfies

$$\parallel d(\boldsymbol{z}, t) \parallel \leq \boldsymbol{\gamma} \parallel \boldsymbol{z} \parallel . \tag{30}$$

Since

$$\begin{aligned}\dot{V}(\boldsymbol{z}) &= \frac{\partial V}{\partial t} + \frac{\partial V}{\partial \boldsymbol{z}} f(\boldsymbol{z}) + \frac{\partial V}{\partial \boldsymbol{z}} d(\boldsymbol{z}, t) \\ &\leq -C_3 \parallel \boldsymbol{z} \parallel^2 + \frac{\partial V}{\partial \boldsymbol{z}} \parallel d(\boldsymbol{z}, t) \parallel \\ &\leq -C_3 \parallel \boldsymbol{z} \parallel^2 + C_4 \gamma \parallel \boldsymbol{z} \parallel^2 \\ &\leq -(C_3 - \gamma C_4) \parallel \boldsymbol{z} \parallel^2,\end{aligned} \tag{31}$$

the system is exponentially stable if γ is small enough to satisfy the bound

$$\gamma \leq \frac{C_3}{C_4}. \tag{32}$$

4.2.2. Stability Proof

The stability proof is based on *Conditional Stability Theorem* (*Theorem 2*). Without loss of generality, lets consider the force control as the first priority task and position control and orientation control as the second and third priority tasks, respectively. The remaining degrees of freedom is also assumed to be exploited in the null space by (26).

Proof of Proposition 1:

By replacing (23)-(19) in the robot dynamics (18), the closed loop dynamics for the main tasks as well as null space dynamics are obtained as

$$-\ddot{\tilde{\boldsymbol{x}}}_f - \boldsymbol{K}_{f,d}\dot{\tilde{\boldsymbol{x}}}_f + \boldsymbol{K}_{f,p}\tilde{\boldsymbol{f}} + \boldsymbol{K}_{f,i}\int_0^t \tilde{\boldsymbol{f}} d\sigma = \bar{\boldsymbol{\Lambda}}_f^{-1}\bar{\boldsymbol{J}}_f^{\#^T}\tilde{\boldsymbol{r}}, \tag{33}$$

$$-\ddot{\tilde{\boldsymbol{x}}} - \boldsymbol{K}_{p,d}\dot{\tilde{\boldsymbol{x}}} + \boldsymbol{K}_{p,p}\tilde{\boldsymbol{x}} = \bar{\boldsymbol{\Lambda}}_p^{-1}\bar{\boldsymbol{J}}_p^{\#^T}\tilde{\boldsymbol{r}}, \tag{34}$$

$$-\dot{\tilde{\boldsymbol{\omega}}}_e - \boldsymbol{K}_{o,d}\bar{\boldsymbol{\omega}}_e + \boldsymbol{K}_{o,p}\boldsymbol{\varepsilon}_{de} = \bar{\boldsymbol{\Lambda}}_o^{-1}\bar{\boldsymbol{J}}_o^{\#^T}\tilde{\boldsymbol{r}}, \tag{35}$$

$$-\bar{\boldsymbol{\Lambda}}_r\dot{\boldsymbol{\nu}} - (\bar{\boldsymbol{\mu}}_r + \boldsymbol{B}_r)\boldsymbol{\nu} + \boldsymbol{Z}_{r-1}\boldsymbol{K}_{r,p}\tilde{\boldsymbol{q}} = \boldsymbol{Z}_{r-1}\boldsymbol{\tau}_{ext}. \tag{36}$$

Additionally, considering estimation error as $\tilde{\boldsymbol{r}} = \boldsymbol{r} + \boldsymbol{\tau}_{ext}$, (22) can be rewritten as

$$\dot{\tilde{\boldsymbol{r}}} + \boldsymbol{K}_{obs}\tilde{\boldsymbol{r}} = \dot{\boldsymbol{\tau}}_{ext}. \tag{37}$$

Consequently, the closed loop dynamics of the system is constructed by (9), (33)-(37) as well as the propagation dynamics [39]

$$\dot{\eta}_{de} = -\frac{1}{2}\boldsymbol{\varepsilon}_{de}^{e^T}\tilde{\boldsymbol{\omega}}_{de}^{e}, \tag{38}$$

$$\dot{\boldsymbol{\varepsilon}}_{de}^{e} = \frac{1}{2}E(\eta_{de}, \varepsilon_{de}^{eT})\tilde{\boldsymbol{\omega}}_{de}^{e}, \tag{39}$$

where $\boldsymbol{\varepsilon}_{de} = \boldsymbol{R}_e\boldsymbol{\varepsilon}_{de}^{e}$, $\tilde{\boldsymbol{\omega}}_{de}^{e} = \boldsymbol{\omega}_{d}^{e} - \bar{\boldsymbol{\omega}}_{e}^{e}$ and $\boldsymbol{\omega}_{d}^{e}$ which is the desired angular velocity is zero. According to the assigned priorities for the stability proof and the definition given in (7), $\bar{\boldsymbol{J}}_f = \bar{\boldsymbol{J}}_1$, $\bar{\boldsymbol{J}}_p = \bar{\boldsymbol{J}}_2$ and $\bar{\boldsymbol{J}}_o = \bar{\boldsymbol{J}}_3$.

The environment stiffness ($\boldsymbol{K}_{env}$) and damping ($\boldsymbol{C}_{env}$) are assumed to be unknown positive quantities. Thus, the applied force on the environment and the desired force are given as follows,

$$\boldsymbol{f}_f = \boldsymbol{K}_{env}(\boldsymbol{x}_f - \boldsymbol{x}_{initial}) + \boldsymbol{C}_{env}\dot{\boldsymbol{x}}_f, \tag{40}$$

$$\boldsymbol{f}_d = \boldsymbol{K}_{env}(\boldsymbol{x}_d - \boldsymbol{x}_{initial}). \tag{41}$$

It should be noted that the desired position $\boldsymbol{x}_d$ is unknown. However, for each desired force it has a specific quantity. One can replace $\tilde{\boldsymbol{f}}$ in (33) with $\boldsymbol{K}_{env}\tilde{\boldsymbol{x}}_f - \boldsymbol{C}_{env}\dot{\boldsymbol{x}}_f$ where $\tilde{\boldsymbol{x}}_f = \boldsymbol{x}_d - \boldsymbol{x}_f$. Since, for independent tasks $\bar{\boldsymbol{x}}_i = \boldsymbol{x}_i$, $\boldsymbol{x}_f$ can be replaced with $\bar{\boldsymbol{x}}_f$ in $\tilde{\boldsymbol{x}}_f$ as well as $\boldsymbol{x}$ with $\bar{\boldsymbol{x}}$ in $\tilde{\boldsymbol{x}}$.

Consequently, the state space vector of the closed loop system is $\boldsymbol{z} = (\dot{\tilde{\boldsymbol{x}}}, \tilde{\boldsymbol{x}}, \dot{\tilde{\boldsymbol{x}}}_f, \tilde{\boldsymbol{x}}_f, \int_0^t \tilde{\boldsymbol{x}}_f d\sigma, \bar{\boldsymbol{\omega}}_e, \boldsymbol{\varepsilon}_{de}, \eta_{de}, \boldsymbol{\nu}, \tilde{\boldsymbol{q}})$. At the first step, stability of the force task in addition to the observer estimation error dynamics are investigated. Equations (33) and (37) can be considered as perturbed linear system

$$\dot{\boldsymbol{z}} = \boldsymbol{A}\boldsymbol{z} + d(\boldsymbol{z}, t), \tag{42}$$

when the external force is assumed to be constant (or slowly time varying). One should consider that this assumption is held during force control since f_f is independent from $\boldsymbol{\tau}_{ext}$ (see (1), (3), (21)). In (42), the perturbation term for nonsingular manipulator configuration is bounded as

$$\| \bar{\boldsymbol{\Lambda}}_f^{-1}\bar{\boldsymbol{J}}_f^{\#^T}\tilde{\boldsymbol{r}} \| \leq \boldsymbol{\gamma} \| \boldsymbol{z} \| . \tag{43}$$

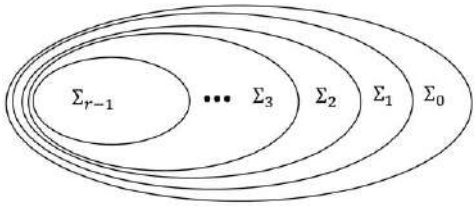

Figure 3: Nested sets used for stability proof in the state space. Σ_0 is the complete and unrestricted state space $\boldsymbol{z}$. By employing the conditional stability theorem for the i-th step, a new subset Σ_i is created where the stability of the next step is studied inside this subset.

Therefore, $d(\boldsymbol{z},t)$ in (42) satisfies (30). By properly choosing the control gains in (23), a negative definite matrix $\boldsymbol{A}$ can be obtained in (30). Hence, the quadratic function

$$V_1(\boldsymbol{z}) = \frac{1}{2}[(\int_0^t \tilde{\boldsymbol{x}}_f d\sigma)^T \ \tilde{\boldsymbol{x}}_f^T \ \dot{\tilde{\boldsymbol{x}}}_f^T \ \tilde{\boldsymbol{r}}^T]\boldsymbol{P}\begin{bmatrix} \int_0^t \tilde{\boldsymbol{x}}_f d\sigma \\ \tilde{\boldsymbol{x}}_f \\ \dot{\tilde{\boldsymbol{x}}}_f \\ \tilde{\boldsymbol{r}} \end{bmatrix}, \tag{44}$$

is exploited in this step where $\boldsymbol{P}$ is a positive definite matrix that fulfills $\boldsymbol{P}\boldsymbol{A} + \boldsymbol{A}^T\boldsymbol{P} = -\boldsymbol{I}$ [16]. Time derivative of (44) along the solutions of (33) and (37) yields

$$\begin{aligned} \dot{V}_1(\boldsymbol{z}) &= \frac{\partial V}{\partial \boldsymbol{z}} f(\boldsymbol{z}) + \frac{\partial V}{\partial \boldsymbol{z}} g(t,\boldsymbol{z}) \\ &= -\dot{\tilde{\boldsymbol{x}}}_f^T \dot{\tilde{\boldsymbol{x}}}_f - \tilde{\boldsymbol{x}}_f^T \tilde{\boldsymbol{x}}_f - (\int_0^t \tilde{\boldsymbol{x}}_f d\sigma)^T (\int_0^t \tilde{\boldsymbol{x}}_f d\sigma) - \tilde{\boldsymbol{r}}^T \tilde{\boldsymbol{r}} \\ &\quad - \bar{\boldsymbol{\Lambda}}_f^{-1} \bar{\boldsymbol{J}}_f^{\#^T} \boldsymbol{\mathcal{H}}(\int_0^t \tilde{\boldsymbol{x}}_f d\sigma, \dot{\tilde{\boldsymbol{x}}}_f, \tilde{\boldsymbol{x}}_f). \end{aligned} \tag{45}$$

where the second line in (45) shows exponential stability of the nominal system and the third line is related to the perturbation term. Since the nominal system in (42) is exponentially stable and (43) holds, by observing *Lemma 3* we realize that (44) and (45) fulfills the first two conditions of *Theorem 2*. For the last condition, asymptotic stability of the system conditionally to set $\Sigma_1 = \{\boldsymbol{z} | \dot{V}_1(\boldsymbol{z}) = 0\} = \{\dot{\tilde{\boldsymbol{x}}}, \tilde{\boldsymbol{x}}, \bar{\boldsymbol{\omega}}_e, \boldsymbol{\varepsilon}_{de}, \boldsymbol{\eta}_{de}, \tilde{\boldsymbol{q}}, \boldsymbol{\nu}, \dot{\tilde{\boldsymbol{x}}}_f = \boldsymbol{0}, \tilde{\boldsymbol{x}}_f = \boldsymbol{0}, \int_0^t \tilde{\boldsymbol{x}}_f d\sigma = \boldsymbol{0}, \tilde{\boldsymbol{r}} = \boldsymbol{0}\}$ must be shown (see Fig. 3). By selecting proper gain matrices in (24) and employing

Lyapunov equation similar to previous step, one can realize the function

$$\begin{aligned} V_2(\boldsymbol{z}) = &\frac{1}{2}\tilde{\boldsymbol{x}}^T(\boldsymbol{K}_{p,d}{\boldsymbol{K}_{p,p}}^{-1} + {\boldsymbol{K}_{p,d}}^{-1}\boldsymbol{K}_{p,p} + {\boldsymbol{K}_{p,d}}^{-1})\tilde{\boldsymbol{x}} \\ &+ \frac{1}{2}\dot{\tilde{\boldsymbol{x}}}^T(\boldsymbol{I} + {\boldsymbol{K}_{p,p}}^{-1})\boldsymbol{K}_{p,d}^{-1}\dot{\tilde{\boldsymbol{x}}} + \dot{\tilde{\boldsymbol{x}}}^T{\boldsymbol{K}_{p,p}}^{-1}\tilde{\boldsymbol{x}}, \end{aligned} \tag{46}$$

which is positive semi-definite within Σ_1. The time derivative of (46) using (34) is simplified as

$$\dot{V}_2(\boldsymbol{z}) = -\dot{\tilde{\boldsymbol{x}}}^T\dot{\tilde{\boldsymbol{x}}} - \tilde{\boldsymbol{x}}^T\tilde{\boldsymbol{x}}. \tag{47}$$

Since (47) is negative semi-definite, to show the asymptotic stability of this subset (Σ_1) using *Theorem 2*, we should investigate asymptotic stability in the subset $\Sigma_2 = \{(\dot{\tilde{\boldsymbol{x}}}, \tilde{\boldsymbol{x}}, \bar{\boldsymbol{\omega}}_e, \boldsymbol{\varepsilon}_{de}, \boldsymbol{\eta}_{de}, \tilde{\boldsymbol{q}}, \boldsymbol{\nu}, \dot{\tilde{\boldsymbol{x}}}_f = \boldsymbol{0}, \tilde{\boldsymbol{x}}_f = \boldsymbol{0}, \int_0^t \tilde{\boldsymbol{x}}_f d\sigma = \boldsymbol{0}, \tilde{\boldsymbol{r}} = \boldsymbol{0}) | \dot{V}_2(\boldsymbol{z}) = 0\}$. Exploiting *Lyapunov* function candidate

$$V_3(\boldsymbol{z}) = \boldsymbol{K}_{o,p}((\eta_{de} - 1)^2 + \boldsymbol{\varepsilon}_{de}^T\boldsymbol{\varepsilon}_{de}) + \frac{1}{2}\bar{\boldsymbol{\omega}}_e^T\bar{\boldsymbol{\omega}}_e \tag{48}$$

and by (38)-(39) we realize

$$\begin{aligned} \dot{V}_3(z) &= 2\boldsymbol{K}_{o,p}((\eta_{de} - 1)\dot{\eta}_{de} + \boldsymbol{\varepsilon}_{de}^T\dot{\boldsymbol{\varepsilon}}_{de}) + \dot{\bar{\boldsymbol{\omega}}}_e^T\bar{\boldsymbol{\omega}}_e \\ &= -\boldsymbol{K}_{o,d}\bar{\boldsymbol{\omega}}_e^T\bar{\boldsymbol{\omega}}_e. \end{aligned} \tag{49}$$

Obviously, $V_3(z)$ and $\dot{V}_3(z)$ satisfy conditional stability prerequisites along the system trajectories. As a result the last subset is realized as $\Sigma_r = \Sigma_3 = \{\tilde{\boldsymbol{q}}, \boldsymbol{\nu}, \boldsymbol{\varepsilon}_{de}, \eta_{de}, \dot{\tilde{\boldsymbol{x}}} = \boldsymbol{0}, \tilde{\boldsymbol{x}} = \boldsymbol{0}, \dot{\tilde{\boldsymbol{x}}}_f = \boldsymbol{0}, \tilde{\boldsymbol{x}}_f = \boldsymbol{0}, \int_0^t \tilde{\boldsymbol{x}}_f d\sigma = \boldsymbol{0}, \tilde{\boldsymbol{r}} = \boldsymbol{0}, \bar{\boldsymbol{\omega}}_e = \boldsymbol{0}\}$. In this set, for the case of non zero accidental external torque ($\boldsymbol{\tau}_{ext}$) and $\boldsymbol{x}(\boldsymbol{q}_d) \neq \boldsymbol{x}_d$, the asymptotic stability can be proven as follows. The equilibrium point for the system in this case is $\{\boldsymbol{q} = \boldsymbol{q}^*, \boldsymbol{\nu} = \boldsymbol{0}, \dot{\tilde{\boldsymbol{x}}} = \boldsymbol{0}, \tilde{\boldsymbol{x}} = \boldsymbol{0}, \dot{\tilde{\boldsymbol{x}}}_f = \boldsymbol{0}, \tilde{\boldsymbol{x}}_f = \boldsymbol{0}, \int_0^t \tilde{\boldsymbol{x}}_f d\sigma = \boldsymbol{0}, \tilde{\boldsymbol{r}} = \boldsymbol{0}, \tilde{\boldsymbol{\omega}} = \boldsymbol{0}, \boldsymbol{\varepsilon}_{de} = \boldsymbol{0}, \eta_{de} = 1\}$ where $\boldsymbol{q}^*$ is a solution of

$$\boldsymbol{Z}_{r-1}(\boldsymbol{K}_{r,p}\tilde{\boldsymbol{q}} - \boldsymbol{\tau}_{ext}) = \boldsymbol{0}, \tag{50}$$

and is compatible with previous tasks. The result locally minimizes the function $||\boldsymbol{K}_{r,p}\tilde{\boldsymbol{q}} - \boldsymbol{\tau}_{ext}||^2$ w.r.t $\boldsymbol{x}_i(\boldsymbol{q}) = \boldsymbol{x}_{i,d}$. More details about computing $\boldsymbol{q}^*$ can be found in [36] and [5]. The proof of asymptotic stability of the equilibrium point of the system is based on the function

$$V_r = \boldsymbol{K}_{o,p}((\eta_{de} - 1)^2 + \boldsymbol{\varepsilon}_{de}^T\boldsymbol{\varepsilon}_{de}) + \frac{1}{2}\boldsymbol{\nu}^T\bar{\boldsymbol{\Lambda}}_r\boldsymbol{\nu} + \frac{1}{2}{\tilde{\boldsymbol{q}}^*}^T\boldsymbol{K}_{r,p}\tilde{\boldsymbol{q}}^*, \tag{51}$$

where $\tilde{\boldsymbol{q}}^* = \boldsymbol{q}^* - \boldsymbol{q}$. Within the set $\boldsymbol{\Sigma}_r$, joint space velocity is $\dot{\boldsymbol{q}} = \bar{\boldsymbol{J}}_r \boldsymbol{\nu}$ and the time derivative of V_r can be computed as

$$\begin{aligned}\dot{V}_r =& -\boldsymbol{\nu}^T(\bar{\boldsymbol{\mu}}_r + \boldsymbol{B}_r)\boldsymbol{\nu} + \boldsymbol{\nu}^T \boldsymbol{Z}_{r-1}\boldsymbol{K}_{r,p}\tilde{\boldsymbol{q}} - \boldsymbol{\nu}^T \boldsymbol{Z}_{r-1}\boldsymbol{\tau}_{ext} \\ & - \boldsymbol{\nu}^T \boldsymbol{Z}_{r-1}\boldsymbol{K}_{r,p}\tilde{\boldsymbol{q}}^* + 2\boldsymbol{K}_{o,p}((\eta_{de}-1)\dot{\eta}_{de} + \boldsymbol{\varepsilon}_{de}^T\dot{\boldsymbol{\varepsilon}}_{de}) \\ =& -\boldsymbol{\nu}^T(\bar{\boldsymbol{\mu}}_r + \boldsymbol{B}_r)\boldsymbol{\nu}.\end{aligned} \tag{52}$$

Note that in the current set $\bar{\boldsymbol{\omega}}_e$ is zero, implying that $\dot{\eta}$ and $\dot{\boldsymbol{\varepsilon}}_{de}$ are null. Considering La Salle's invariance principal, the state of the system converges to the largest invariant set with $\boldsymbol{\nu} = \boldsymbol{0}$ in Σ_r. By observing the system closed loop equations beside (50), the invariant set is realized as $\{\boldsymbol{q} = \boldsymbol{q}^*, \boldsymbol{\nu} = \boldsymbol{0}, \dot{\tilde{\boldsymbol{x}}} = \boldsymbol{0}, \tilde{\boldsymbol{x}} = \boldsymbol{0}, \dot{\tilde{\boldsymbol{x}}}_f = \boldsymbol{0}, \tilde{\boldsymbol{x}}_f = \boldsymbol{0}, \int_0^t \tilde{\boldsymbol{x}}_f d\sigma = \boldsymbol{0}, \tilde{\boldsymbol{r}} = \boldsymbol{0}, \tilde{\boldsymbol{\omega}} = \boldsymbol{0}, \boldsymbol{\varepsilon}_{de} = \boldsymbol{0}, \eta_{de} = 1\}$. It is noteworthy that there is another equilibrium point for the system as $\{\boldsymbol{q} = \boldsymbol{q}^*, \boldsymbol{\nu} = \boldsymbol{0}, \dot{\tilde{\boldsymbol{x}}} = \boldsymbol{0}, \tilde{\boldsymbol{x}} = \boldsymbol{0}, \dot{\tilde{\boldsymbol{x}}}_f = \boldsymbol{0}, \tilde{\boldsymbol{x}}_f = \boldsymbol{0}, \int_0^t \tilde{\boldsymbol{x}}_f d\sigma = \boldsymbol{0}, \tilde{\boldsymbol{r}} = \boldsymbol{0}, \boldsymbol{\omega}_e = \boldsymbol{0}, \boldsymbol{\varepsilon}_{de} = \boldsymbol{0}, \eta_{de} = -1\}$ which is unstable. This can be shown by taking a small perturbation around this equilibrium point. Let $\eta_{de} = -1 + \sigma$ and $\sigma > 0$ and consider that unit quaternion parameters are constrained as

$$\eta^2 + \boldsymbol{\varepsilon}^T\boldsymbol{\varepsilon} = 1. \tag{53}$$

Perturbed V_r simplifies to $V_{r_\sigma} = 4\boldsymbol{K}_{o,p} - 2\sigma\boldsymbol{K}_{o,p}$ while V_r for the equilibrium point is $V_{r,eq} = 4\boldsymbol{K}_{o,p}$. By (52), V_r is decreasing and will never return to $V_{r,eq}$ from $V_{r,\sigma}$. Thus, we can infer that this equilibrium point is unstable (similar analysis can be found in [4]).

When $\boldsymbol{\tau}_{ext} = \boldsymbol{0}$, the asymptotic stability is preserved while the system converges to new equilibrium point for $\boldsymbol{q}$ and the equilibrium set is $\{\boldsymbol{q} = \boldsymbol{q}_d, \boldsymbol{\nu} = \boldsymbol{0}, \dot{\tilde{\boldsymbol{x}}} = \boldsymbol{0}, \tilde{\boldsymbol{x}} = \boldsymbol{0}, \dot{\tilde{\boldsymbol{x}}}_f = \boldsymbol{0}, \tilde{\boldsymbol{x}}_f = \boldsymbol{0}, \int_0^t \tilde{\boldsymbol{x}}_f d\sigma = \boldsymbol{0}, \tilde{\boldsymbol{r}} = \boldsymbol{0}, \boldsymbol{\omega}_e = \boldsymbol{0}, \boldsymbol{\varepsilon}_{de} = \boldsymbol{0}, \eta_{de} = 1\}$.

Therefore, by virtue of *Theorem 2*, Σ_3 is asymptotically stable. Subsequently, the third condition of this theorem in the subsets Σ_2 and Σ_1 is satisfied and thus the asymptotic stability of the equilibrium point of the system is realized.

Remark 1: An alternative scheme to show the system stability is to replace

V_1 with two positive semi-definite functions: V_{obs} and V_f. Consider

$$V_{obs} = \frac{1}{2}\tilde{\boldsymbol{r}}^T\tilde{\boldsymbol{r}}, \tag{54}$$

and its time derivative along the system trajectory as

$$\dot{V}_{obs} = -\dot{\tilde{\boldsymbol{r}}}^T\boldsymbol{K}_{obs}\dot{\tilde{\boldsymbol{r}}}, \tag{55}$$

at the first step. Hence, the stability analysis of the system should be discussed in the subset $\Sigma_{obs} = \{\boldsymbol{z}|\dot{V}_{obs}(\boldsymbol{z}) = 0\} = \{\dot{\tilde{\boldsymbol{x}}}, \tilde{\boldsymbol{x}}, \bar{\boldsymbol{\omega}}_e, \boldsymbol{\varepsilon}_{de}, \boldsymbol{\eta}_{de}, \tilde{\boldsymbol{q}}, \boldsymbol{\nu}, \dot{\tilde{\boldsymbol{x}}}_f, \tilde{\boldsymbol{x}}_f, \int_0^t \tilde{\boldsymbol{x}}_f d\sigma, \tilde{\boldsymbol{r}} = \boldsymbol{0}\}$. One can propose proper V_f for showing the stability of the force control task by using Lyapunov equation. To this end, matrix $\boldsymbol{P}$ in $\boldsymbol{P}\boldsymbol{A} + \boldsymbol{A}^T\boldsymbol{P} = -\boldsymbol{I}$ should be computed according to $\boldsymbol{A}$ which is realized from (33) in the subset Σ_{obs}. This way, the *Lemma* 3 is not employed anymore. The rest of the stability analysis is the same as previous.

Remark 2: If multiple similar tasks are considered for manipulation, the similar structure of V_2, V_3 and V_f can be employed for the tasks in the realized subsets. In the other hand, stability analysis of the hybrid tasks is possible through the summation of the corresponding Lyapunov functions. Finally, the absence of any type of the tasks does not disturb the procedure and just omits the relevant step.

Remark 3: According to (20), if the considered tasks are dependent, the lower priority task is realized as much as possible in the sense of least-squares. In other words, the norm of $||\ddot{\tilde{\boldsymbol{x}}} - \ddot{\boldsymbol{x}}_c + \bar{\boldsymbol{J}}_i M^{-1}\boldsymbol{\tau}_{ext}||$ is minimized subjected to the higher priority tasks. Since the observer performance is independent of the allocated priorities, the effect of $\boldsymbol{\tau}_{ext}$ will be certainly compensated.

Remark 4: Because of the using pseudo-inverse in the solution, singularity may arise when the manipulator moves from a nonsingular to a singular configuration. Damped Least-Squares (DLS) method is usually employed to treat this condition. Using DLS in the second-order kinematic control is discussed in [3]. However, occurring this case is not common in the regulation tasks which are considered here.

5. Experimental Evaluation

The proposed approach is verified experimentally on a 7DOF KUKA LWR robot arm. Various robot control approaches are investigated through this manipulator [1, 24, 13]. Moreover, a six axis Force/Torque sensor (ATI Mini-45) is mounted at the end-effector of the robot to measure the forces applied on the tip (Fig. 4).

Each scenario comprises two prioritized tasks in addition to the compliance behavior at the third level. Control algorithms are executed through fast research interface library (FRI) on a remote PC. Three experimental scenarios are devised. Corresponding command accelerations are used in (19) to obtain the desired behavior for the tasks along with null space compliance.

5.1. Case I

In this case, hybrid force-position control is considered as the first priority task and the position control is set as the second priority task. This combination of the tasks is useful for both humanoid robots and manipulators during complex manipulations. Humanoids can preserve their stability by proper force control on their foots (and even another point of contacts) while executing other tasks using their redundancy (examples can be found in [38] and [19]). The application of robot manipulators for Minimally Invasive Surgery (MIS) is another example where a robot needs to apply accurate force by the surgical tools at the end-effector while passing through a small incision.

In the current experiment, the initial robot configuration is $\boldsymbol{q}_d = \{0, \pi/6, 0, -\pi/2, 0, \pi/3, 0\}$ and the desired task is to apply $f_z = -5\ N$ force with the end effector tip to a specific point of platform located at $\boldsymbol{x}_{d_1} = [-0.5378\ 0]$. The second task is to preserve the end of the 5-th arm initial position in the XY plane during manipulation. Equations (23), (24) and (26) are used to obtain the desired behavior while external forces are applied to the robot body by a human. In order to protect the robot and force sensor from unexpected happenings, soft panels are used as the environment (Fig. 4).

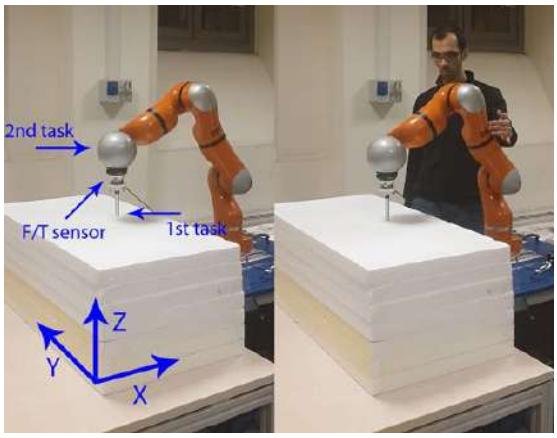

Figure 4: Case I: The experimental setup during manipulation.

The performance of the controller is illustrated in the Fig. 5. Five intervals are shown in the the figures related to this case (Fig. 5 and Fig. 6). "I" is the interval which robot moves toward the platform for applying force. During intervals "A", "B", "C" and "D", external forces are applied to the various points of the robot body by a human (see Fig. 4). However, during applying force by the tip of the end effector, undesired external forces exist in X and Y directions too (see Fig. 6). The magnitude of the external interaction estimated by both the robot internal torque sensor and by using (21) are shown in Fig. 6. The difference between these two vectors is related to the Z direction force at the tip of the end-effector. Note that in (21), the intentional torques are omitted from the residual vector.

Fig. 5 shows that the force magnitude converges to the desired value rapidly when it reaches the platform. Considering the interaction intervals shown in the Fig. 5, it can be seen that the force and position errors are negligible during the external interaction.

For the sake of studying the effect of using the observer in our control scheme, this scenario is repeated with the same gains for the task space and null space acceleration command while the external torque compensation is omitted in (23) and (24). The results are shown in Fig. 7 and Fig. 8. Without using

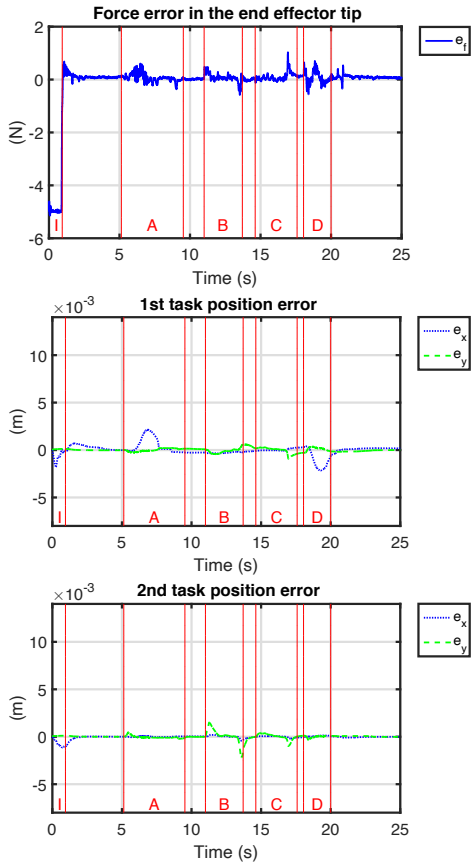

Figure 5: Case I: First task force error (Top) and position error (Middle). Second task position error (Bottom). "I" corresponds to the initial interval where robot moves toward the platform. "A", "B", "C" and "D" show the Intervals where human applies external interaction on the robot body.

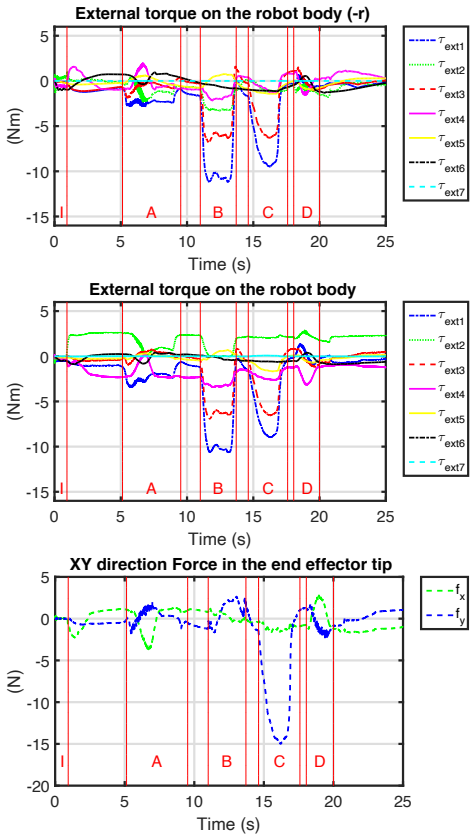

Figure 6: Case I: External torques applied to the robot body computed by (21) (Top) and by internal torque sensors (Middle). The force magnitude at the end effector in X and Y directions (f_x and f_y) evaluated by the force sensor (Bottom).

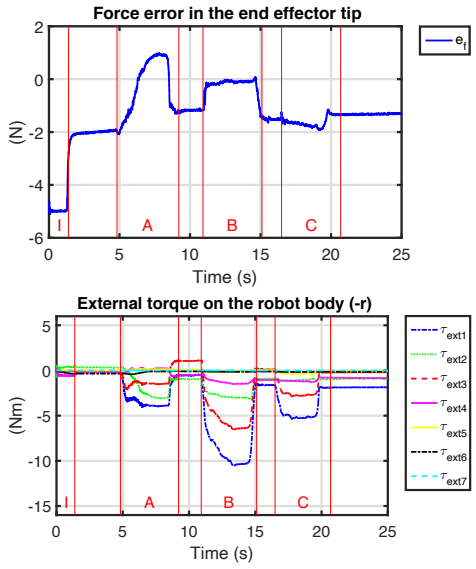

Figure 7: Case I: Experimental results without using observer: First task force error (Top), External torque applied to the robot body (Bottom).

the observer, the force convergence rate decreases significantly when the end effector interacts with the platform (Fig. 7). We tried to apply external forces almost to the same points of the robot in both cases. As it can be seen from the Fig. 7 and Fig. 6, the maximum amount of the external torques are almost the same.

Without using the observer, the force magnitude variations in the interaction intervals ("A", "B" and "C" in Fig. 7) are significantly higher than the case with controller-observer (Fig. 5). Furthermore, convergence rate to the desired value is too slow in comparison with the proposed approach. Position control errors in both first and second priority tasks increase by omitting the observer and it is non-null not only during the interaction phase but also after that (Fig. 6). It is noteworthy that the error increases much more for the second priority task in comparison to the first priority task.

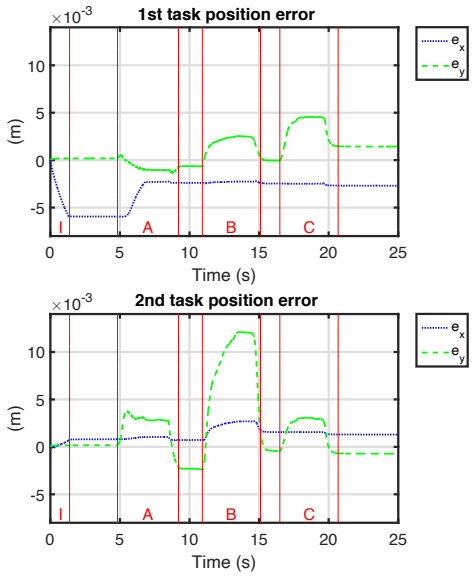

Figure 8: Case I: Experimental results without using observer: First task position error (Top), Second task position error (Bottom).

5.2. Case II

Preserving the desired orientation is a critical issue, especially in robotic surgery and visual servoing. Consider the case where a surgery tool mounted at the end-effector passes through an incision point in an MIS scenario. Meanwhile, it should preserve specified orientation for example to ensure the safety of neighbor organs, apply force in the specific direction or provide a special view in the endoscopic camera which is mounted at the robot end effector (Fig. 9). The current case studies the approach functionality in such scenarios.

In this set of experiments, the performance of the schemes for orientation control is studied by considering the end-effector orientation and the end of the 5-th arm XY position as the first task (Fig. 10). The second task is the end effector position in Z direction. Robot initial configuration is $\boldsymbol{q}_i = \{0, \pi/6, 0, -\pi/2, \pi/6, -\pi/3, 0\}$ and it is commanded to show an impedance behavior when any external forces are applied to its body. The control command is computed by substituting (24)-(26) in (19).

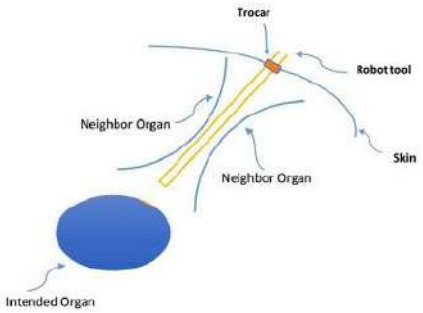

Figure 9: Sample scenario for orientation control; a surgery tool mounted at the end-effector passes through an incision point in a MIS scenario.

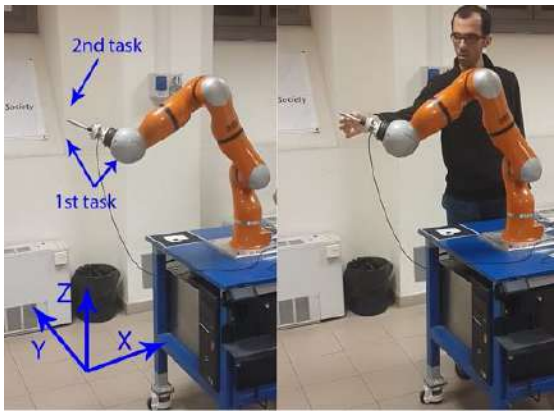

Figure 10: Case II: Snapshots of the experimental setup during manipulation.

The results are shown in Fig. 11 and Fig. 12. According to the subsection 4.2.2, η_{de} and ϵ_{de} should converge to 1 and $\mathbf{0}$, respectively. As it can be seen in Fig. 11, the deviation of the orientation parameters from the desired values is negligible during the interaction phases ("A", "B", "C" and "D"). Position tasks errors are significantly small and converge to zero when the external interaction is constant (see Fig. 12).

5.3. Case III

In the last case study, the corresponding XYZ position of the end effector, XY position of the end of the 5-th arm and constant joint space configuration

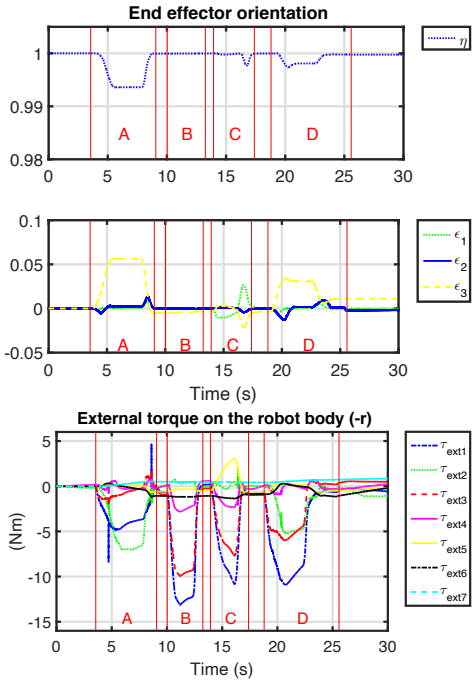

Figure 11: Case II: Quaternion parameters (Top), External torques applied to the robot body (Bottom).

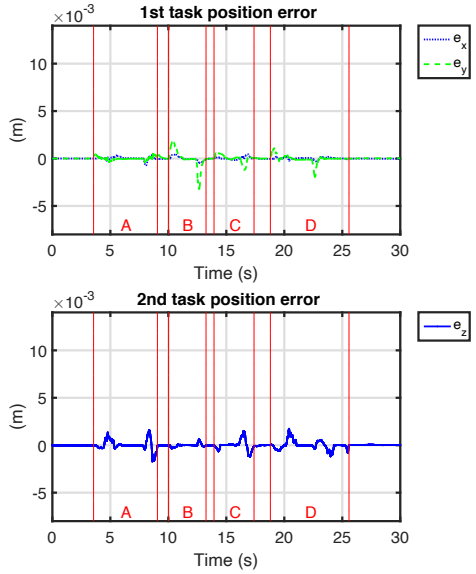

Figure 12: Case II: First task position error (Top), Second task position error (Bottom).

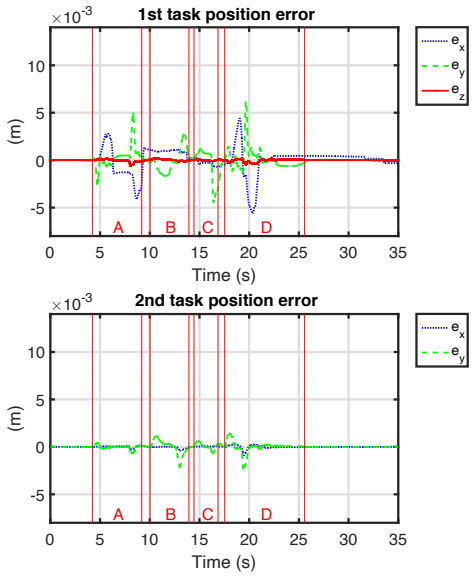

Figure 13: Case III: First task position error (Top), Second task position error (Bottom).

$q_d = \{0, \pi/6, 0, -\pi/2, 0, \pi/3, 0\}$ are considered as the tasks in the hierarchy. Fig. 13 and Fig. 14 show the same performance of the controller when the tasks are the same in the first and second priorities. Robot reaction in the task space to the external interactions is similar to the previous cases and the error converges to zero right after the interaction with the robot body. The last interaction interval, in this case, consists of two consecutive external interactions in two different positions and directions.

5.4. Discussion

Experimental results show that by using the proposed controller-observers along with the priority allocation method, system stability is guaranteed and manipulation performance is enhanced remarkably. The method performance in various hybrid force-position control (*Case I*), hybrid position-orientation control (*Case II*) is considerable. In *Case I*, the results demonstrate that the controller-observer efficiency is not limited to the interaction phase and enhances the manipulation accuracy all over the experiment. Moreover, em-

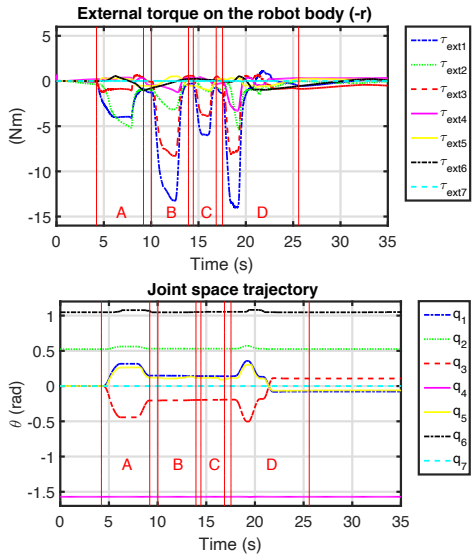

Figure 14: Case III: External torques applied to the robot body (Top), Joint space trajectory (Bottom).

ploying uncertain inertial and Coriolis/centrifugal matrices or even neglecting Coriolis/centrifugal force do not make the method performance unacceptable. This issue is proven by multiple experiments carried out in similar cases by the authors and is in accordance with the report in [36] for one position regulation task. All the model inaccuracies are computed in $\boldsymbol{\tau}_{ext}$ which is compensated in the control law.

During the experiments, external forces are applied to the different points on the robot body. The robot configuration changes compliantly when the interaction position is a bit far from the task accomplishment location (such as the one shown on the right side of Fig. 4). Interaction occurred in the intervals "A" and "D" in all the experiments are reporting this type of interactions. Considering joint space trajectory in Fig. 14, robot configuration is adopted compliantly to the external force in the null space of the higher priority tasks. Meanwhile, applying similar external force in the exact location of the defined tasks (during interaction intervals "B" and "C") does not change the robot configuration and causes a bigger external torque on the robot body which the

proposed controller method is robust to that. Similar behavior was seen for robot joint space trajectory as the last task in other cases. Hence, we can conclude that all the intentions of the method for facilitating accurate and friendly accomplishment of various complex tasks at different priority level are met in the experiments.

It is noteworthy to consider that the control torque and the exchanged force during the physical interaction may increase significantly if the amount of the external force exceeds an acceptable limit which depends on the robot structure, tasks, *etc.*. A solution for this problem is suspending the main manipulation tasks and showing a compliance behavior through all degrees of freedom. In this situation, by replacing $\boldsymbol{Z}_{r-1}$ with $(n \times n)$ identity matrix in (26) and other equations along with omitting other tasks from (19) joint space impedance control can be obtained.

6. Conclusion

In this work, a novel controller-observer was proposed to accomplish various tasks at different priority levels. To this end, a new priority assignment scheme was investigated for priority allocation. The controller guarantees accurate execution of multiple tasks besides compliant behavior in the null space during the interaction on the robot body. The proposed observer estimates the external interaction torques without using torque sensor and redundant degrees of freedom are exploited to realize a compliant behavior during the interaction. By using the proposed method, the disturbance effect in the main tasks is reduced significantly and in the case of no accidental interaction, the main task performance is enhanced considerably. Consequently, the robot can be utilized safely for accurate manipulation in human environments. Stability analysis of the system including force, position and orientation tasks control at different priority levels is given. The stability analysis scheme is in general form and covers various combinations of the tasks. Finally, the analytical analyses are confirmed by implementing the method in different cases on a 7DOF robot arm.

7. References

[1] A. Ajoudani, N. G. Tsagarakis, and A. Bicchi. Tele-impedance: Preliminary results on measuring and replicating human arm impedance in tele operated robots. In *2011 IEEE International Conference on Robotics and Biomimetics*, pages 216–222, Dec 2011.

[2] K. Bouyarmane and A. Kheddar. Using a multi-objective controller to synthesize simulated humanoid robot motion with changing contact configurations. In *2011 IEEE/RSJ International Conference on Intelligent Robots and Systems*, pages 4414–4419, Sept 2011.

[3] F. Caccavale, S. Chiaverini, and B. Siciliano. Second-order kinematic control of robot manipulators with jacobian damped least-squares inverse: theory and experiments. *IEEE/ASME Transactions on Mechatronics*, 2(3):188–194, Sep 1997.

[4] Fabrizio Caccavale, Ciro Natale, Bruno Siciliano, and Luigi Villani. Resolved-acceleration control of robot manipulators: A critical review with experiments. *Robotica*, 16(05):565–573, 1998.

[5] Pyung-Hun Chang. A closed-form solution for inverse kinematics of robot manipulators with redundancy. 1987.

[6] C. Collette, A. Micaelli, C. Andriot, and P. Lemerle. Dynamic balance control of humanoids for multiple grasps and non coplanar frictional contacts. In *2007 7th IEEE-RAS International Conference on Humanoid Robots*, pages 81–88, Nov 2007.

[7] R. Corteso and M. Dominici. Robot force control on a beating heart. *IEEE/ASME Transactions on Mechatronics*, 22(4):1736–1743, Aug 2017.

[8] Alessandro De Luca and Raffaella Mattone. Sensorless robot collision detection and hybrid force/motion control. In *Robotics and Automation, 2005. ICRA 2005. Proceedings of the 2005 IEEE International Conference on*, pages 999–1004. IEEE, 2005.

[9] Fabrizio Flacco and Alessandro De Luca. A reverse priority approach to multi-task control of redundant robots. In *Intelligent Robots and Systems (IROS 2014), 2014 IEEE/RSJ International Conference on*, pages 2421–2427. IEEE, 2014.

[10] Fabrizio Flacco, Alessandro De Luca, and Oussama Khatib. Prioritized multi-task motion control of redundant robots under hard joint constraints. In *Intelligent Robots and Systems (IROS), 2012 IEEE/RSJ International Conference on*, pages 3970–3977. IEEE, 2012.

[11] Ping Hsu, John Mauser, and Shankar Sastry. Dynamic control of redundant manipulators. *Journal of Robotic Systems*, 6(2):133–148, 1989.

[12] B. Iggidr, A. Kalitine and R. Outbib. Semidefinite lyapunov functions stability and stabilization. *Mathematics of Control, Signals and Systems*, 9(2):95–106, 1996.

[13] L. Jin and S. Li. Distributed task allocation of multiple robots: A control perspective. *IEEE Transactions on Systems, Man, and Cybernetics: Systems*, 48(5):693–701, May 2018.

[14] Seul Jung, T. C. Hsia, and R. G. Bonitz. Force tracking impedance control of robot manipulators under unknown environment. *IEEE Transactions on Control Systems Technology*, 12(3):474–483, May 2004.

[15] S. B. Kesner and R. D. Howe. Force control of flexible catheter robots for beating heart surgery. In *2011 IEEE International Conference on Robotics and Automation*, pages 1589–1594, May 2011.

[16] Hassan K Khalil and JW Grizzle. *Nonlinear systems*, volume 3. Prentice hall New Jersey, 1996.

[17] M. Khatib, K. A. Khudir, and A. De Luca. Visual coordination task for human-robot collaboration. In *2017 IEEE/RSJ International Conference on Intelligent Robots and Systems (IROS)*, pages 3762–3768, Sept 2017.

[18] O. Khatib. A unified approach for motion and force control of robot manipulators: The operational space formulation. *IEEE Journal on Robotics and Automation*, 3(1):43–53, February 1987.

[19] O. Khatib and S. Y. Chung. Suprapeds: Humanoid contact-supported locomotion for 3d unstructured environments. In *2014 IEEE International Conference on Robotics and Automation (ICRA)*, pages 2319–2325, May 2014.

[20] Oussama Khatib. Inertial properties in robotic manipulation: An object-level framework. *The international journal of robotics research*, 14(1):19–36, 1995.

[21] Mingxing Liu, Yang Tan, and Vincent Padois. Generalized hierarchical control. *Autonomous Robots*, 40(1):17–31, 2016.

[22] A. De Luca and G. Oriolo. Nonholonomic behavior in redundant robots under kinematic control. *IEEE Transactions on Robotics and Automation*, 13(5):776–782, Oct 1997.

[23] Alessandro De Luca, Massimo Ferri, Giuseppe Oriolo, and Paolo Robuffo Giordano. Visual servoing with exploitation of redundancy: An experimental study. In *Robotics and Automation, 2008. ICRA 2008. IEEE International Conference on*, pages 3231–3237. IEEE, 2008.

[24] A. Mashayekhi, S. Behbahani, F. Ficuciello, and B. Siciliano. Analytical stability criterion in haptic rendering: The role of damping. *IEEE/ASME Transactions on Mechatronics*, 23(2):596–603, April 2018.

[25] Michael Mistry, Jun Nakanishi, and Stefan Schaal. Task space control with prioritization for balance and locomotion. In *Intelligent Robots and Systems, 2007. IROS 2007. IEEE/RSJ International Conference on*, pages 331–338. IEEE, 2007.

[26] Jun Nakanishi, Rick Cory, Michael Mistry, Jan Peters, and Stefan Schaal. Operational space control: A theoretical and empirical comparison. *The International Journal of Robotics Research*, 27(6):737–757, 2008.

[27] N. V. Navkar, Z. Deng, D. J. Shah, K. E. Bekris, and N. V. Tsekos. Visual and force-feedback guidance for robot-assisted interventions in the beating heart with real-time mri. In *2012 IEEE International Conference on Robotics and Automation*, pages 689–694, May 2012.

[28] D. Nicolis, A. M. Zanchettin, and P. Rocco. Constraint-based and sensorless force control with an application to a lightweight dual-arm robot. *IEEE Robotics and Automation Letters*, 1(1):340–347, Jan 2016.

[29] Yonghwan Oh, Wankyun Chung, and Youngil Youm. Extended impedance control of redundant manipulators based on weighted decomposition of joint space. *Journal of Robotic Systems*, 15(5):231–258, 1998.

[30] C. Ott. *Cartesian Impedance Control of Redundant and Flexible-Joint Robots*. Springer Tracts in Advanced Robotics. Springer Berlin Heidelberg, 2008.

[31] Christian Ott, Alexander Dietrich, and Alin Albu-Schäffer. Prioritized multi-task compliance control of redundant manipulators. *Automatica*, 53:416–423, 2015.

[32] Jaeheung Park and Oussama Khatib. Multi-link multi-contact force control for manipulators. In *Robotics and Automation, 2005. ICRA 2005. Proceedings of the 2005 IEEE International Conference on*, pages 3613–3618. IEEE, 2005.

[33] M. P. Polverini, R. Rossi, G. Morandi, L. Bascetta, A. M. Zanchettin, and P. Rocco. Performance improvement of implicit integral robot force control through constraint-based optimization. In *2016 IEEE/RSJ International Conference on Intelligent Robots and Systems (IROS)*, pages 3368–3373, Oct 2016.

[34] H. Sadeghian, L. Villani, Z. Kamranian, and A. Karami. Visual servoing with safe interaction using image moments. In *Intelligent Robots and Systems (IROS), 2015 IEEE/RSJ International Conference on*, pages 5479–5485, Sept 2015.

[35] Hamid Sadeghian, Luigi Villani, Mehdi Keshmiri, and Bruno Siciliano. Dynamic multi-priority control in redundant robotic systems. *Robotica*, 31(07):1155–1167, 2013.

[36] Hamid Sadeghian, Luigi Villani, Mehdi Keshmiri, and Bruno Siciliano. Task-space control of robot manipulators with null-space compliance. *Robotics, IEEE Transactions on*, 30(2):493–506, 2014.

[37] F. Sato, T. Nishii, J. Takahashi, Y. Yoshida, M. Mitsuhashi, and D. Nenchev. Experimental evaluation of a trajectory/force tracking controller for a humanoid robot cleaning a vertical surface. In *2011 IEEE/RSJ International Conference on Intelligent Robots and Systems*, pages 3179–3184, Sept 2011.

[38] L. Sentis, J. Park, and O. Khatib. Compliant control of multicontact and center-of-mass behaviors in humanoid robots. *IEEE Transactions on Robotics*, 26(3):483–501, June 2010.

[39] Bruno Siciliano, Lorenzo Sciavicco, and Luigi Villani. *Robotics : modelling, planning and control*. Advanced Textbooks in Control and Signal Processing. Springer, London, 2010.

[40] Bruno Siciliano and Jean-Jacques E Slotine. A general framework for managing multiple tasks in highly redundant robotic systems. In *Advanced Robotics, 1991.'Robots in Unstructured Environments', 91 ICAR., Fifth International Conference on*, pages 1211–1216. IEEE, 1991.

[41] A. Winkler and J. Such. Force controlled contour following on unknown objects with an industrial robot. In *2013 IEEE International Symposium on Robotic and Sensors Environments (ROSE)*, pages 208–213, Oct 2013.

[42] N. Zemiti, G. Morel, T. Ortmaier, and N. Bonnet. Mechatronic design of a new robot for force control in minimally invasive surgery. *IEEE/ASME Transactions on Mechatronics*, 12(2):143–153, April 2007.

accident2.png

c1_comf_2.jpg

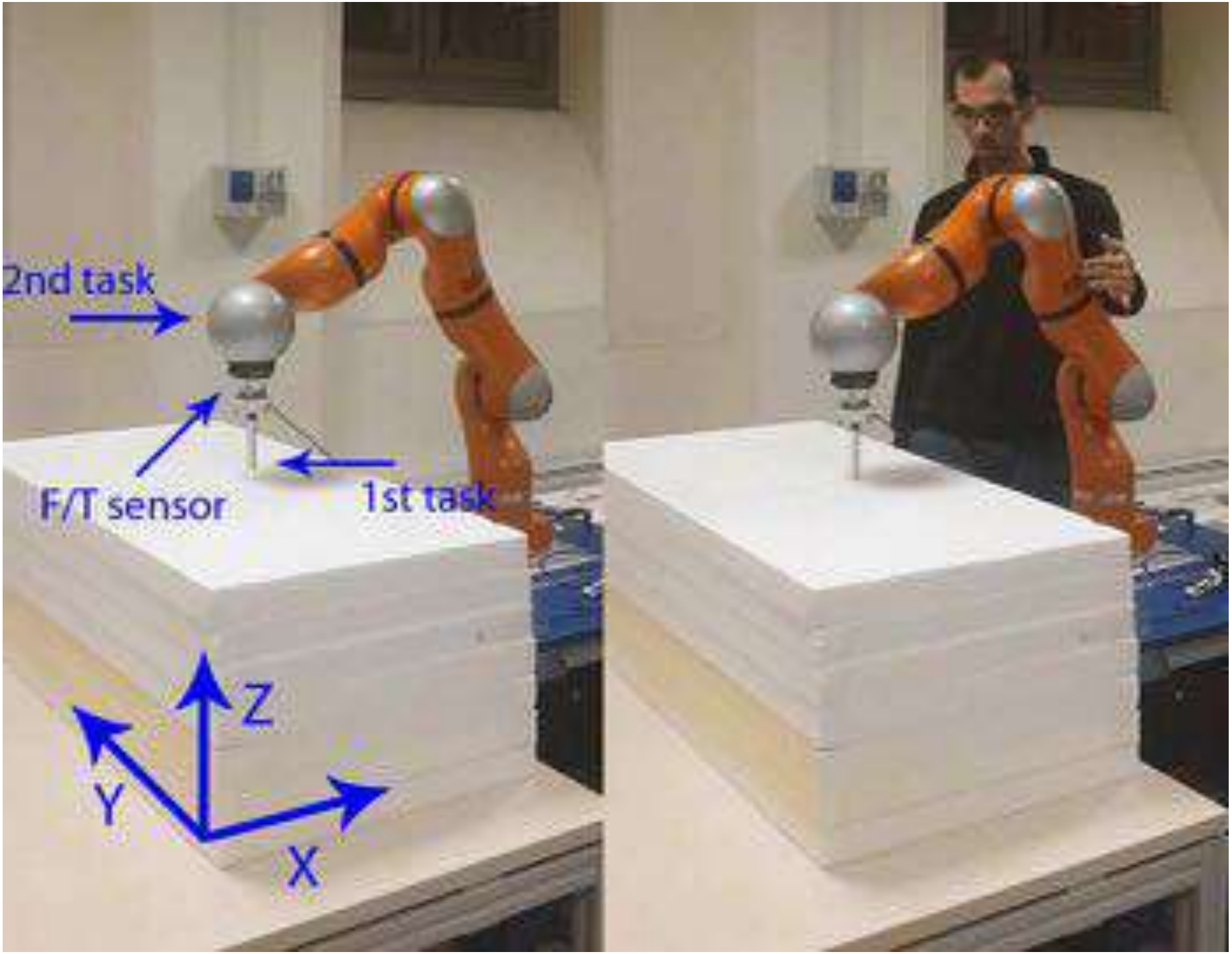

c2_comp_comf2-2.jpg

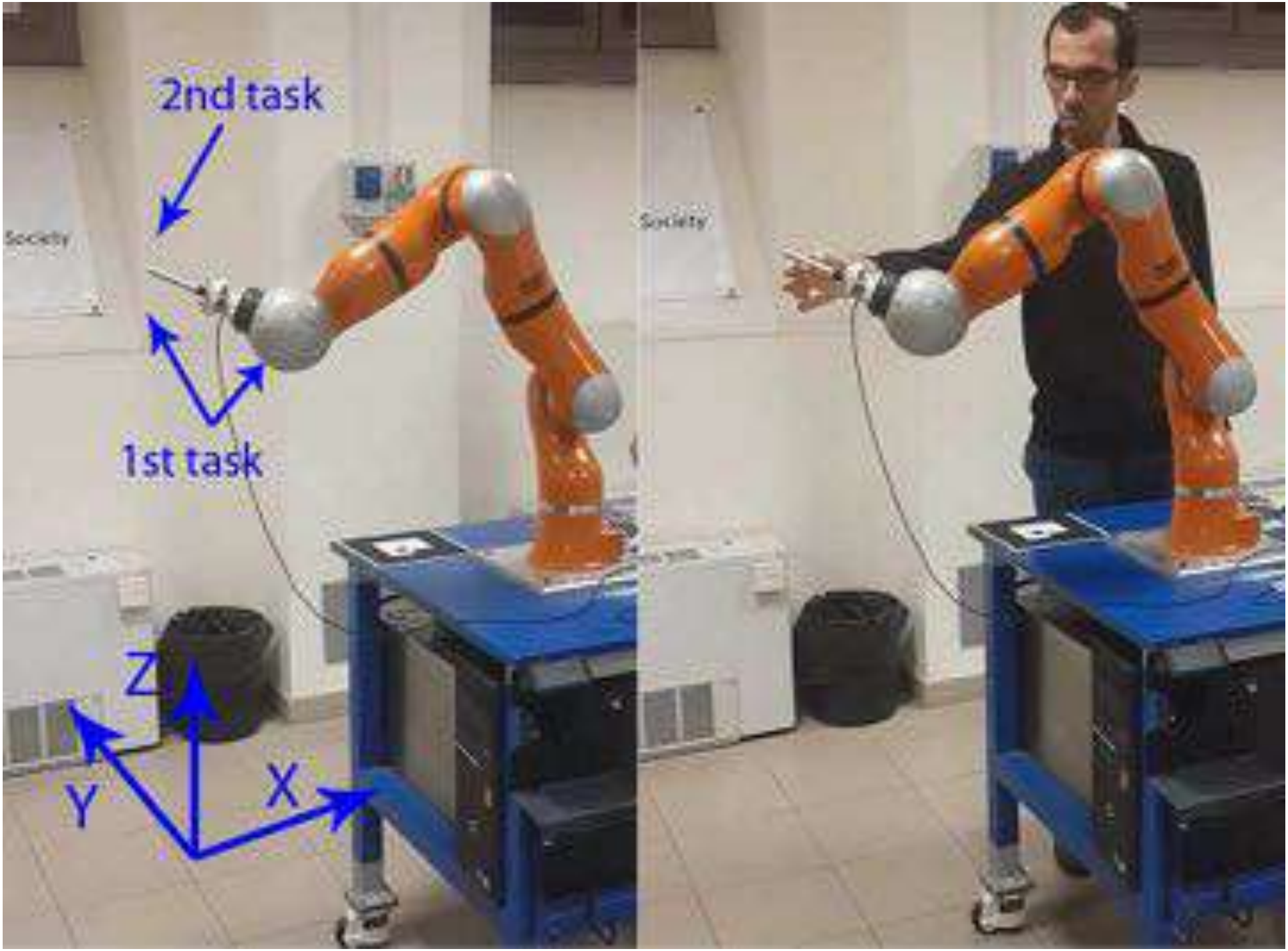

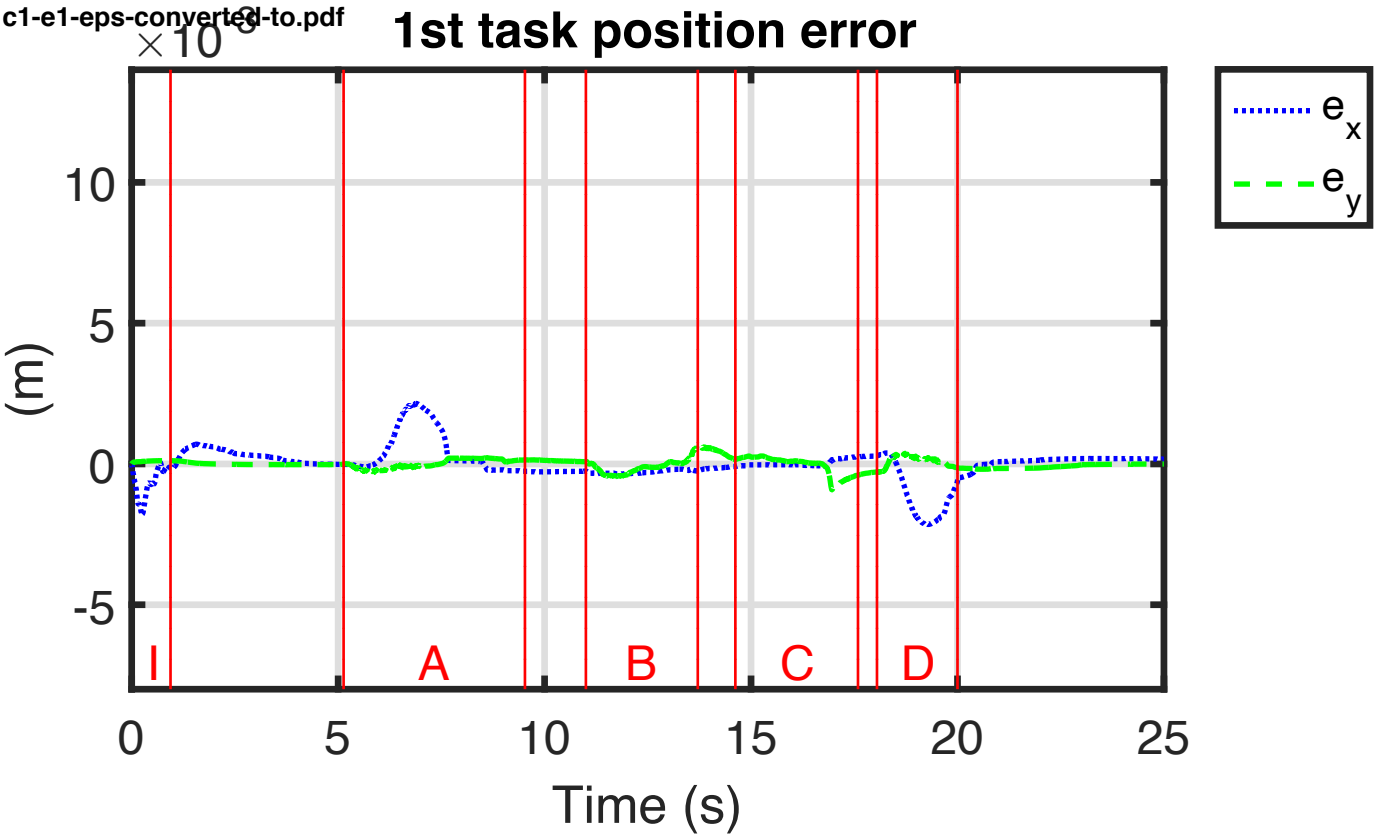


c1-e2-eps-converted-to.pdf
2nd task position error
×10^-3
10
5
0
-5
(m)
I
A
B
C
D
0
5
10
15
20
25
Time (s)
e_x
e_y

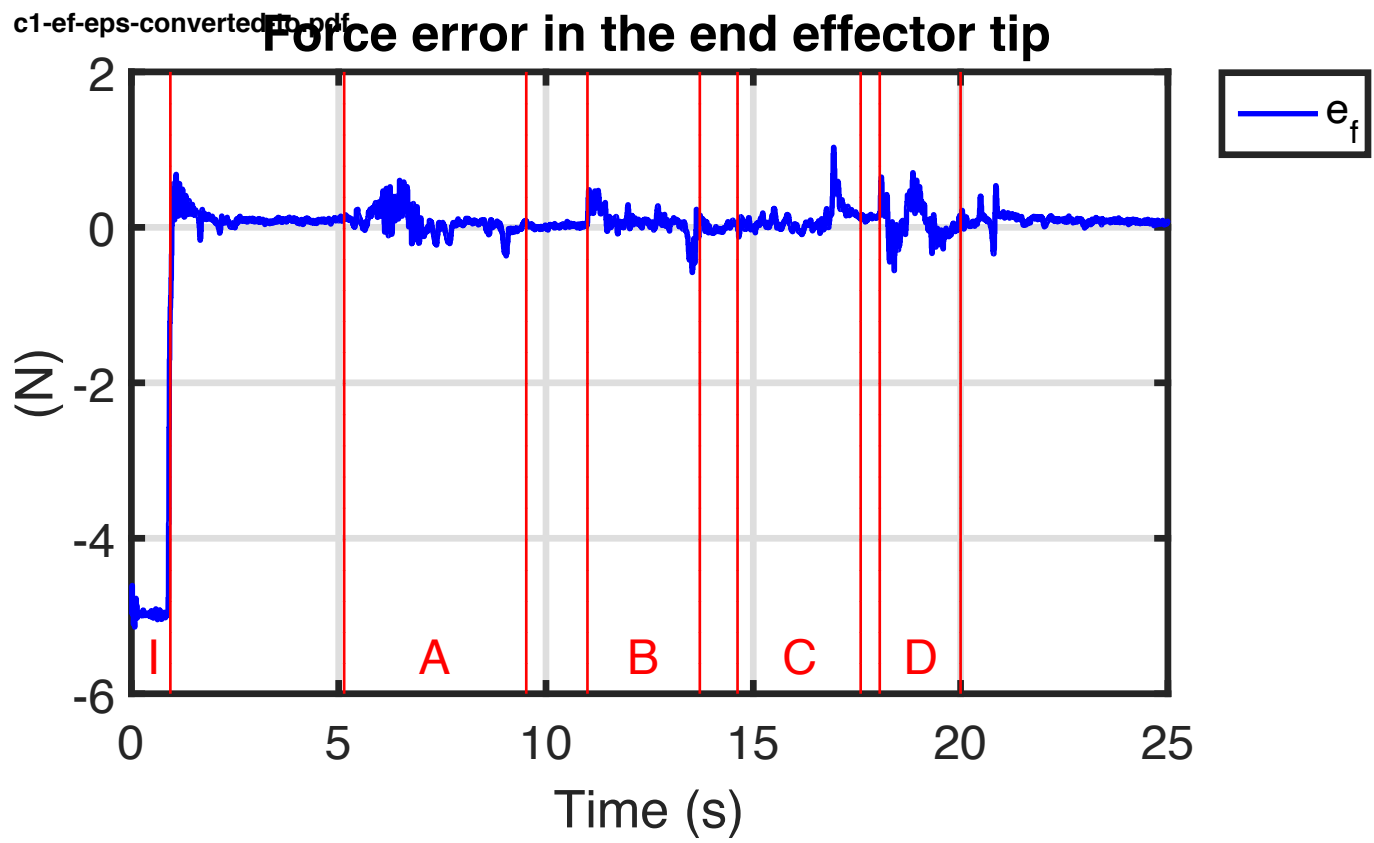
c1-ef-eps-converted-to.pdf
Force error in the end effector tip
2
0
-2
-4
-6
(N)
0
5
10
15
20
25
Time (s)
I
A
B
C
D
e_f

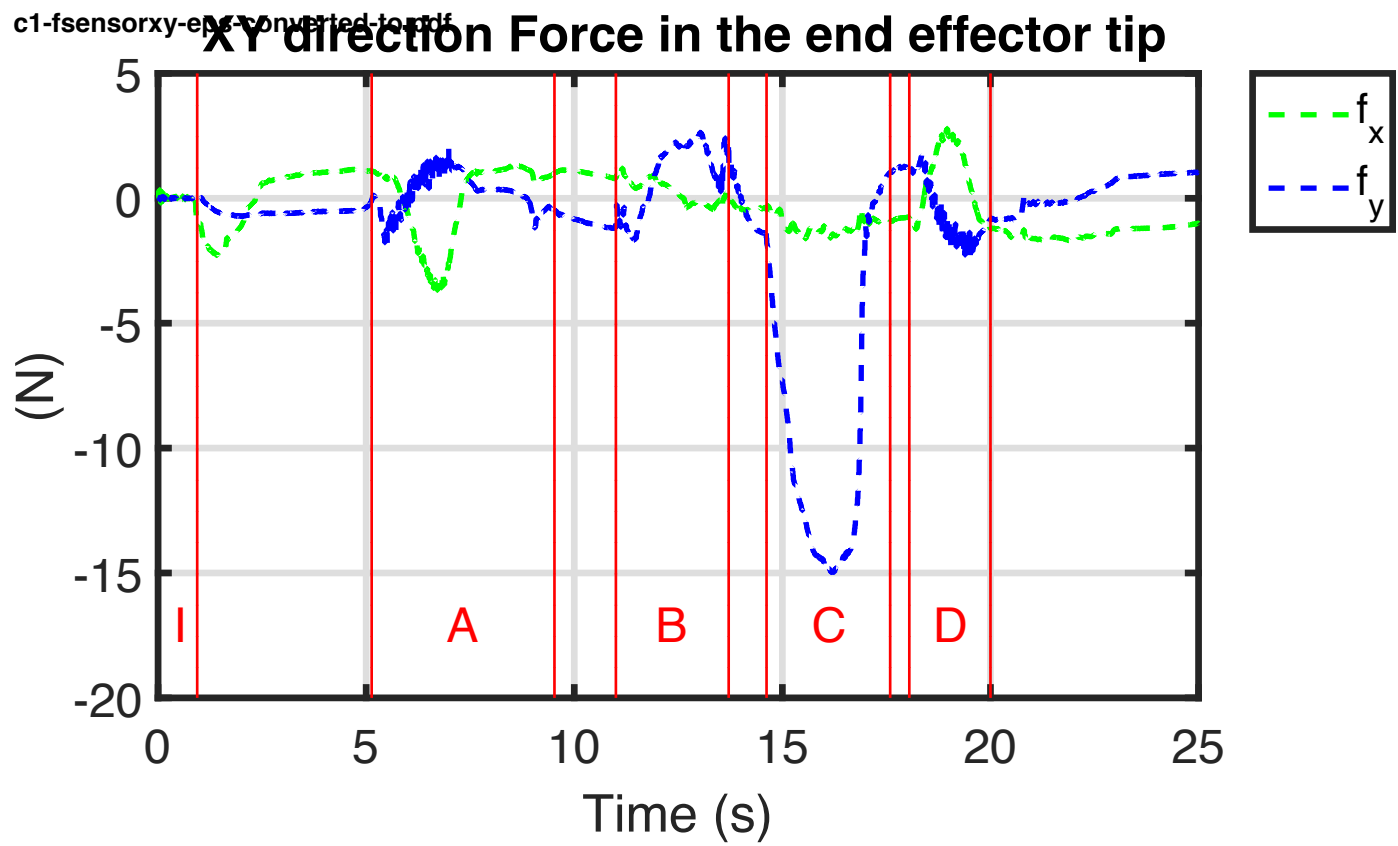
c1-fsensorxy-eps-converted-to.pdf
XY direction Force in the end effector tip
5
0
-5
-10
-15
-20
(N)
I
A
B
C
D
0
5
10
15
20
25
Time (s)
f x
f y

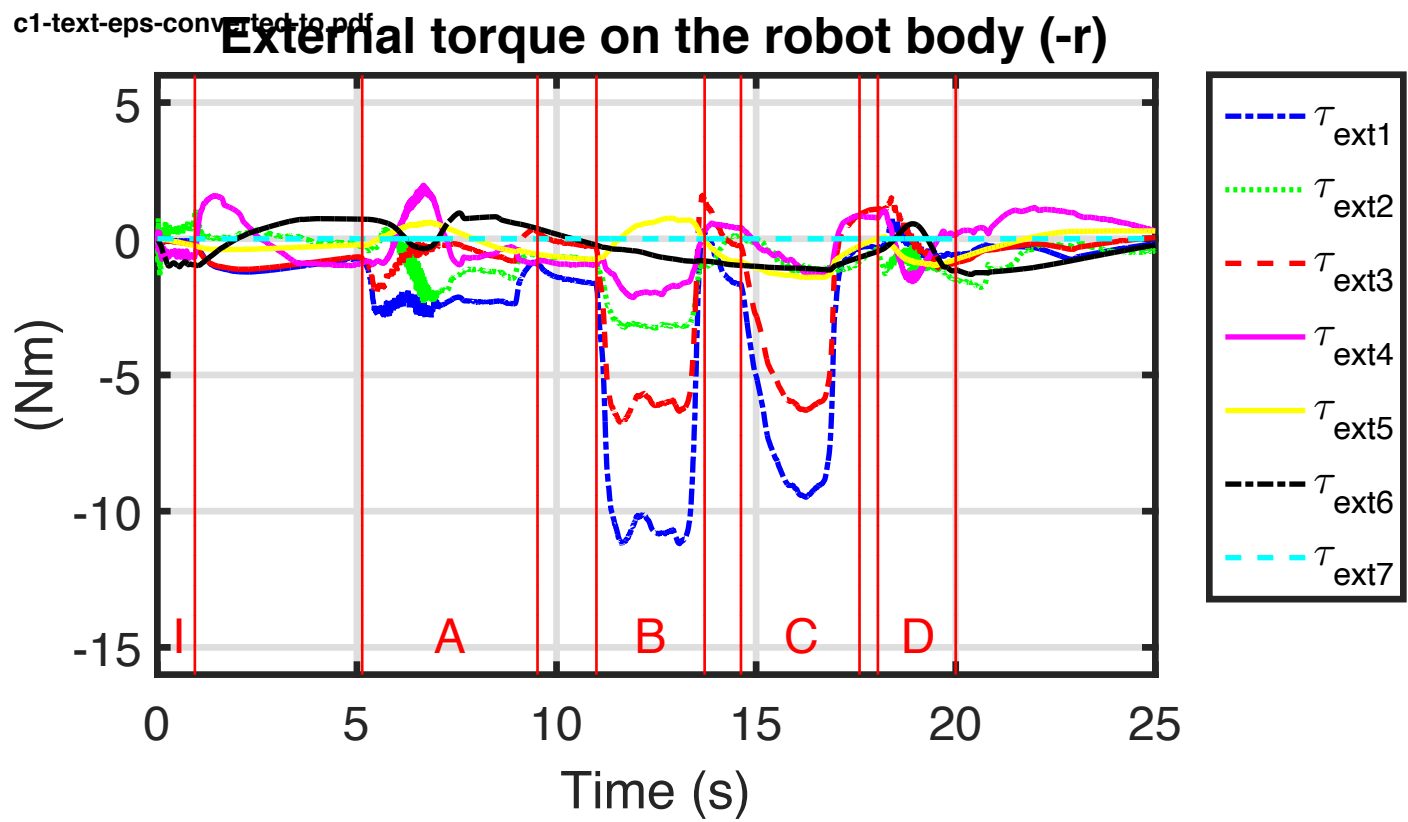

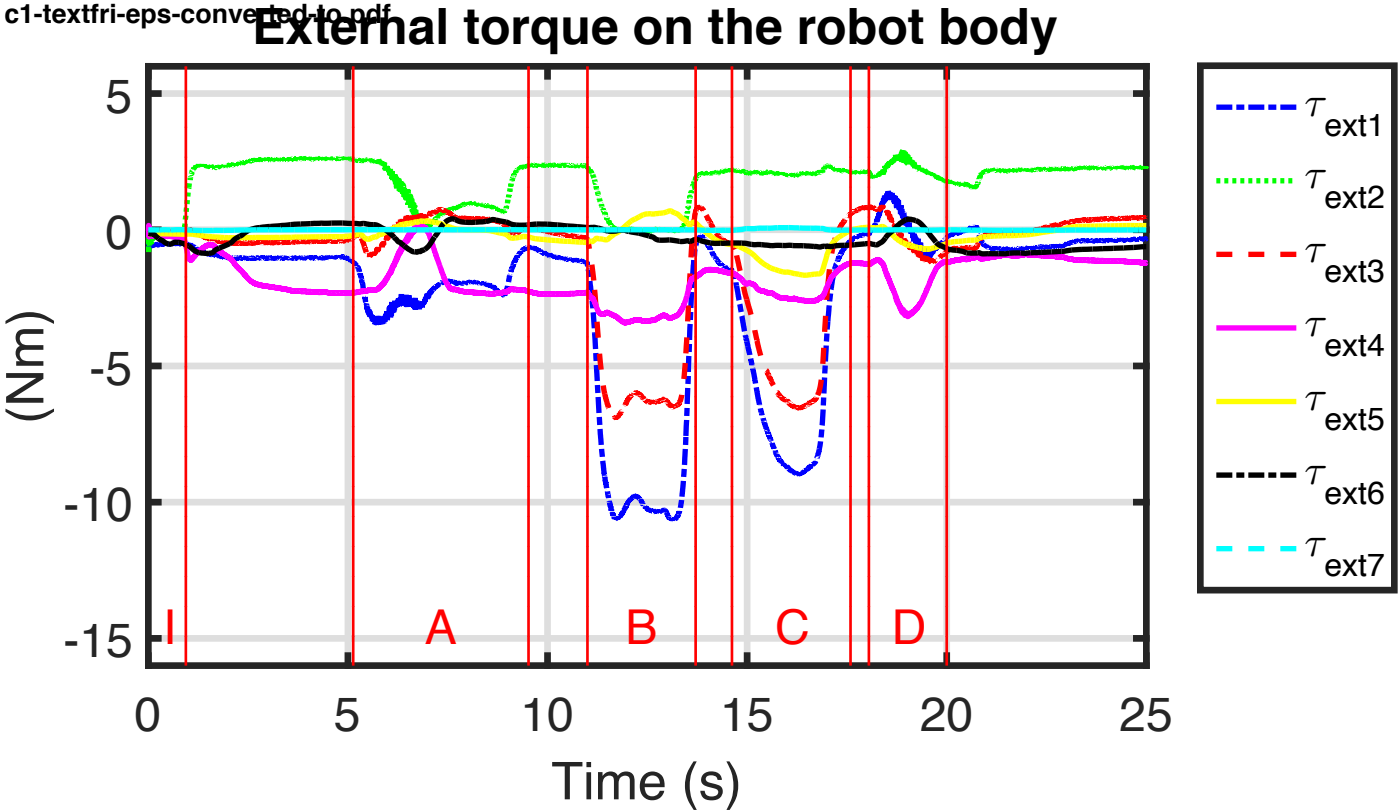

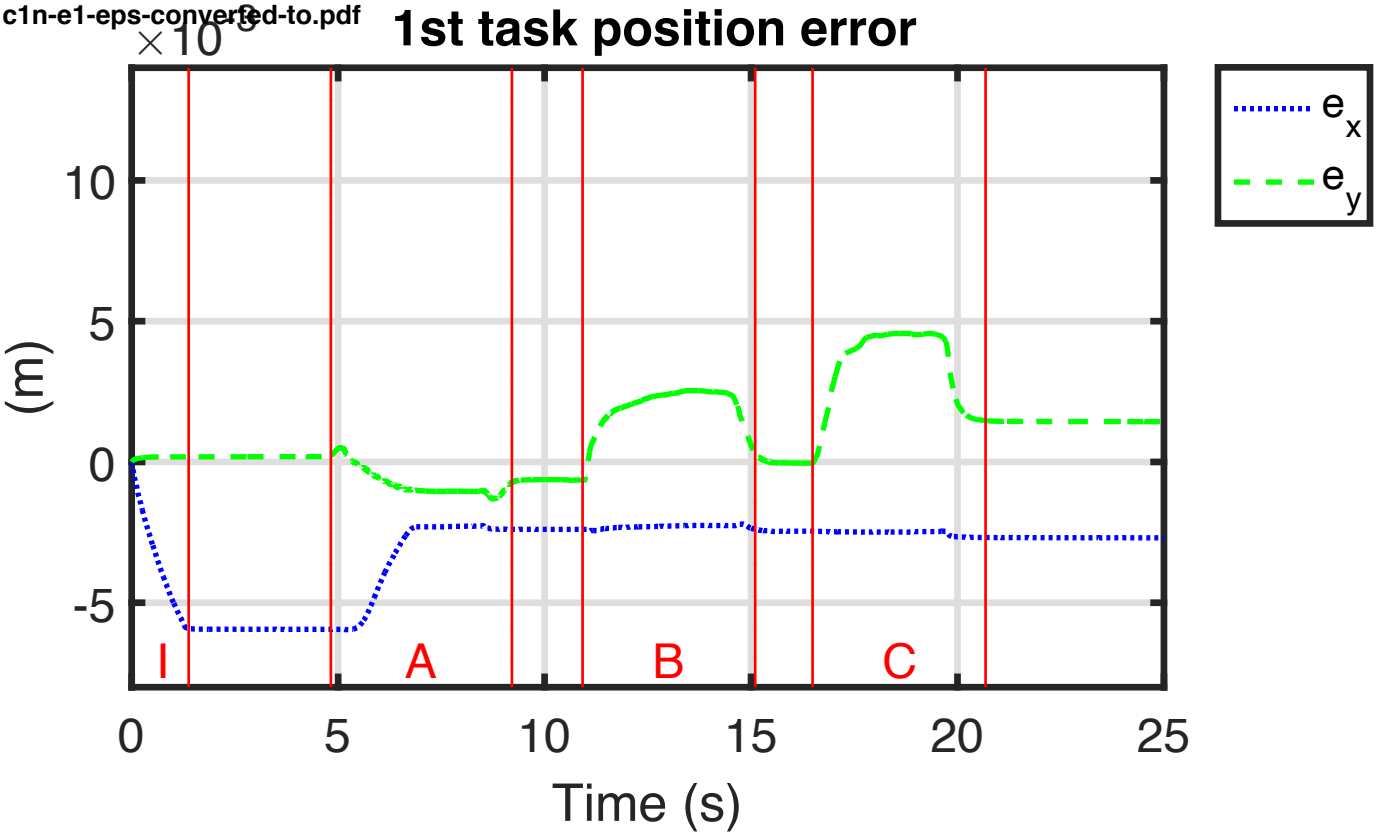


c1n-e2-eps-converted-to.pdf
2nd task position error
×10^-3
10
5
0
-5
(m)
I
A
B
C
0
5
10
15
20
25
Time (s)
e_x
e_y

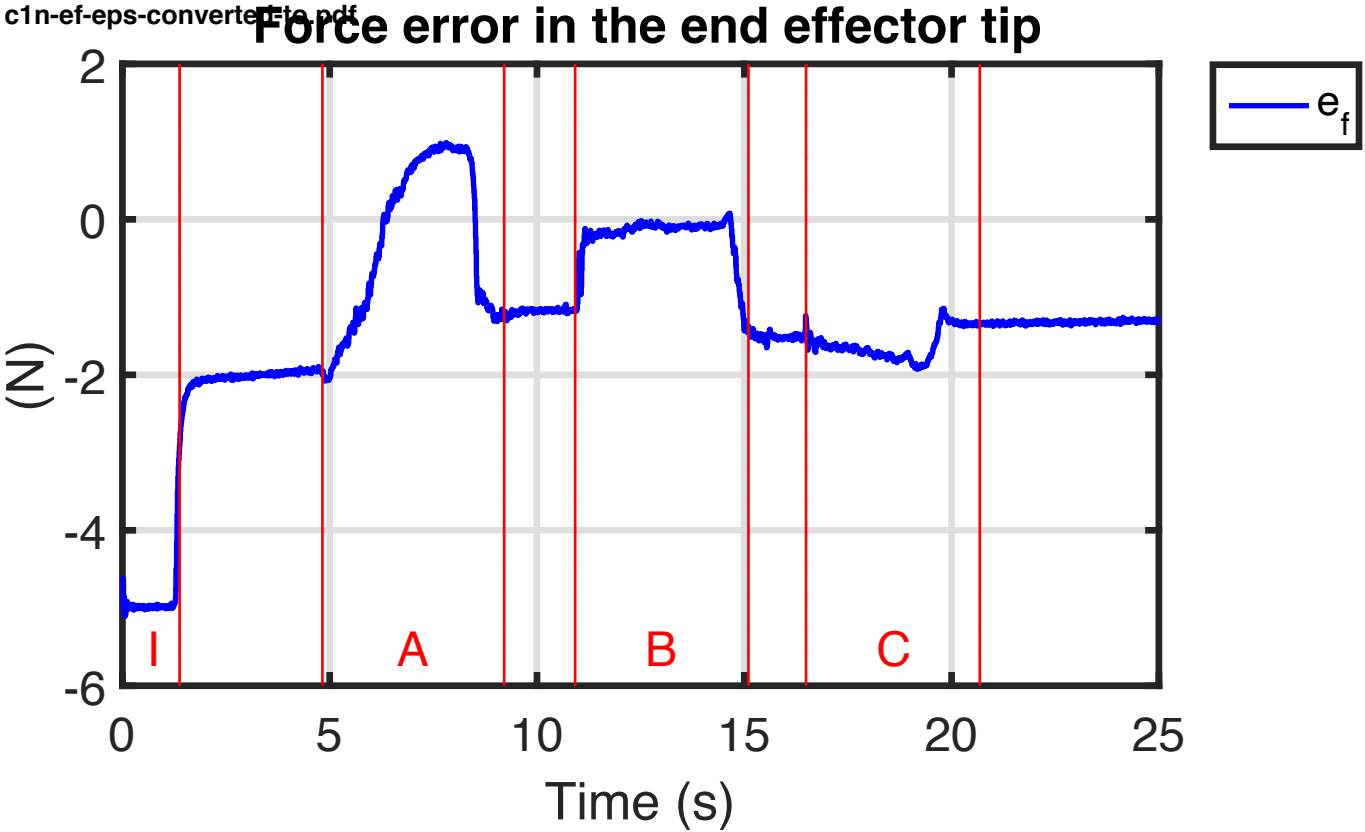

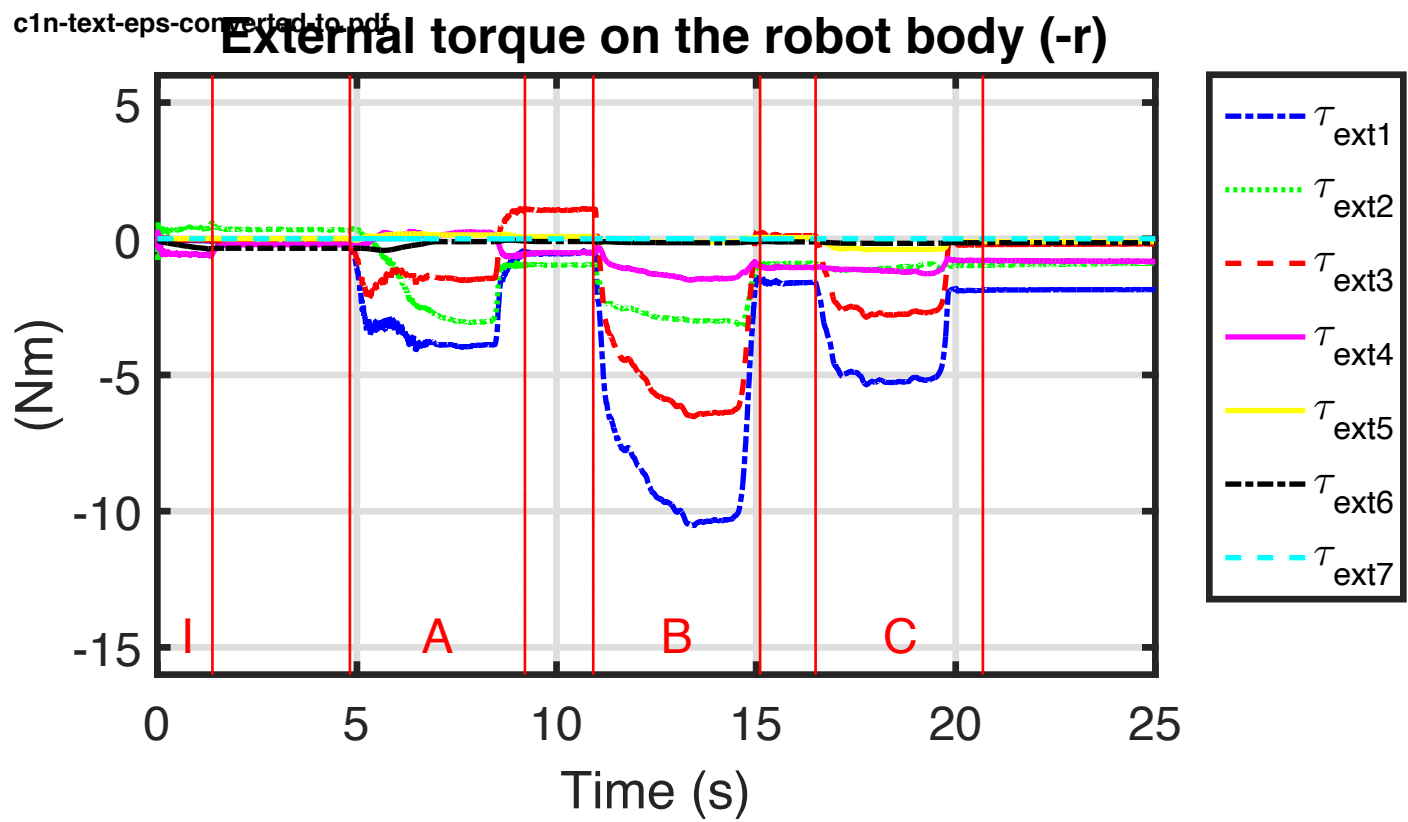

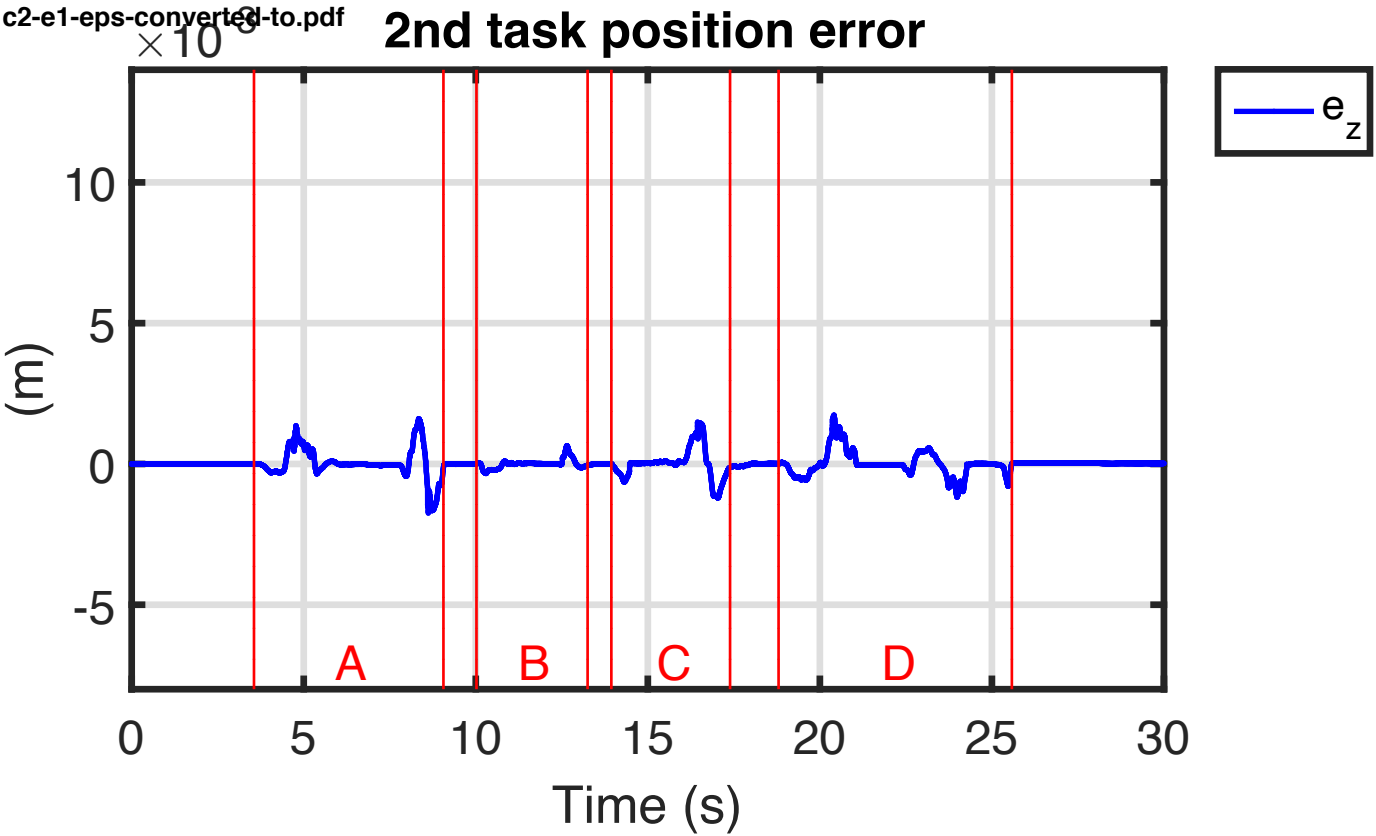

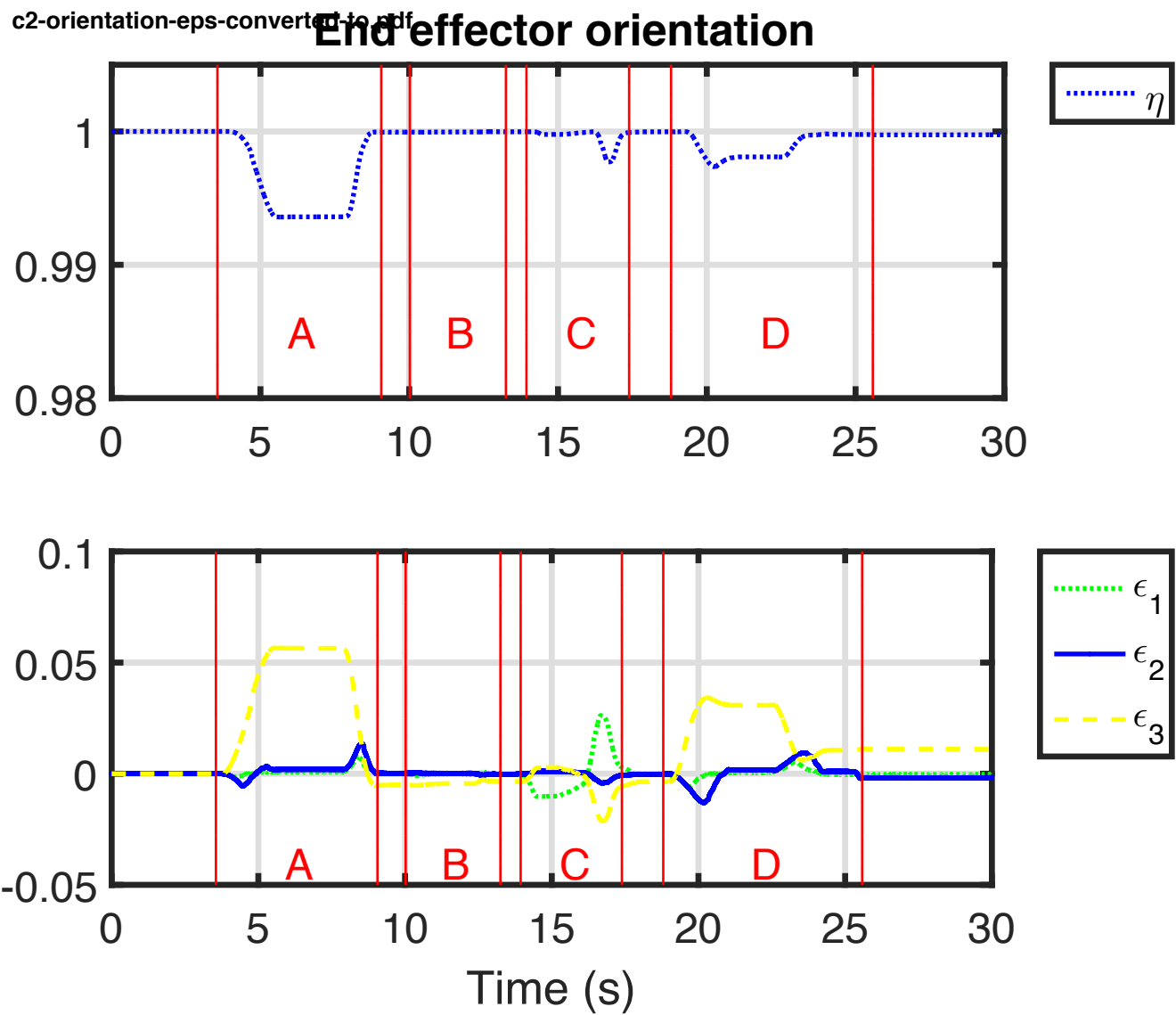

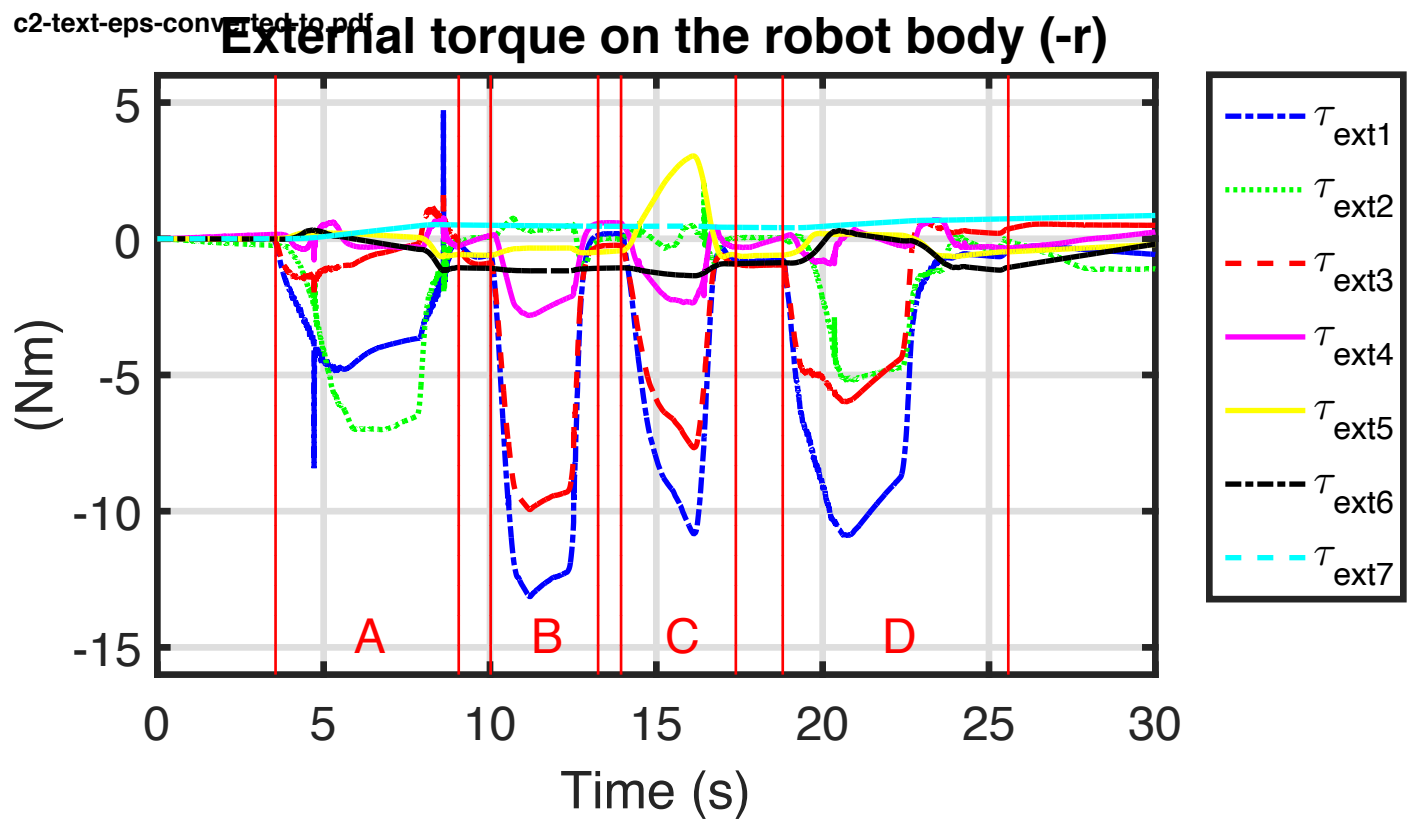

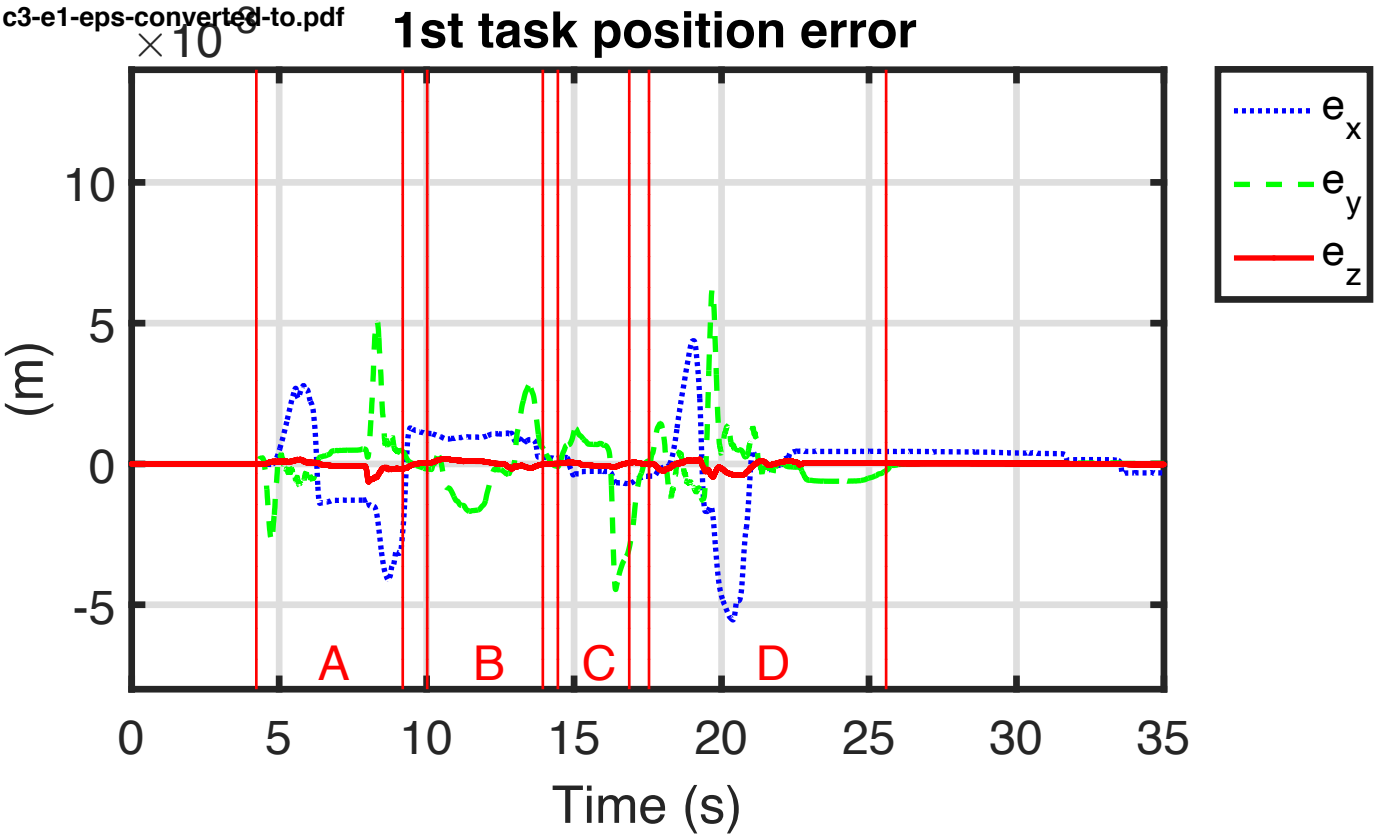

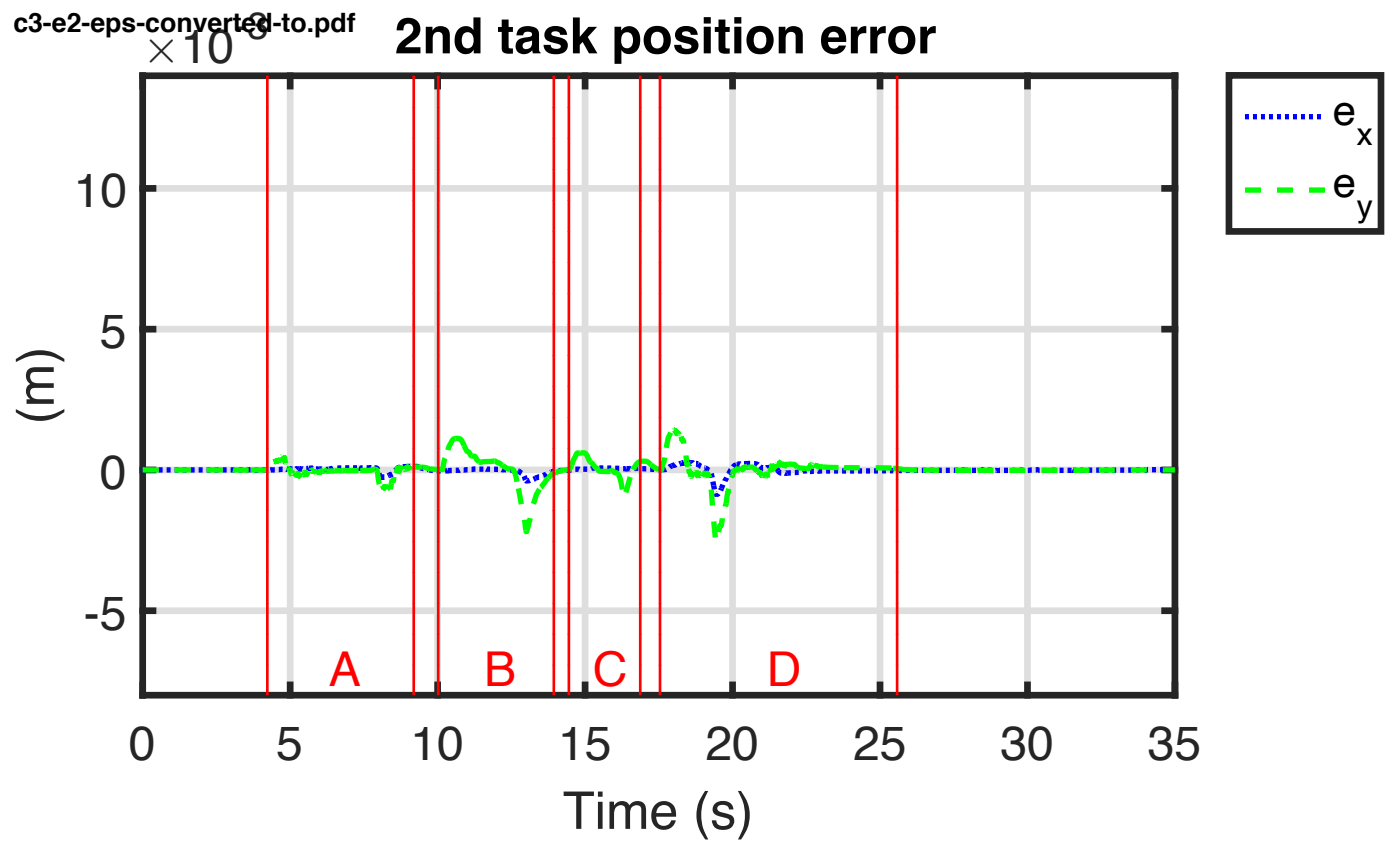
c3-e2-eps-converted-to.pdf
2nd task position error
×10^-3
10
5
0
-5
(m)
A
B
C
D
0
5
10
15
20
25
30
35
Time (s)
e_x
e_y

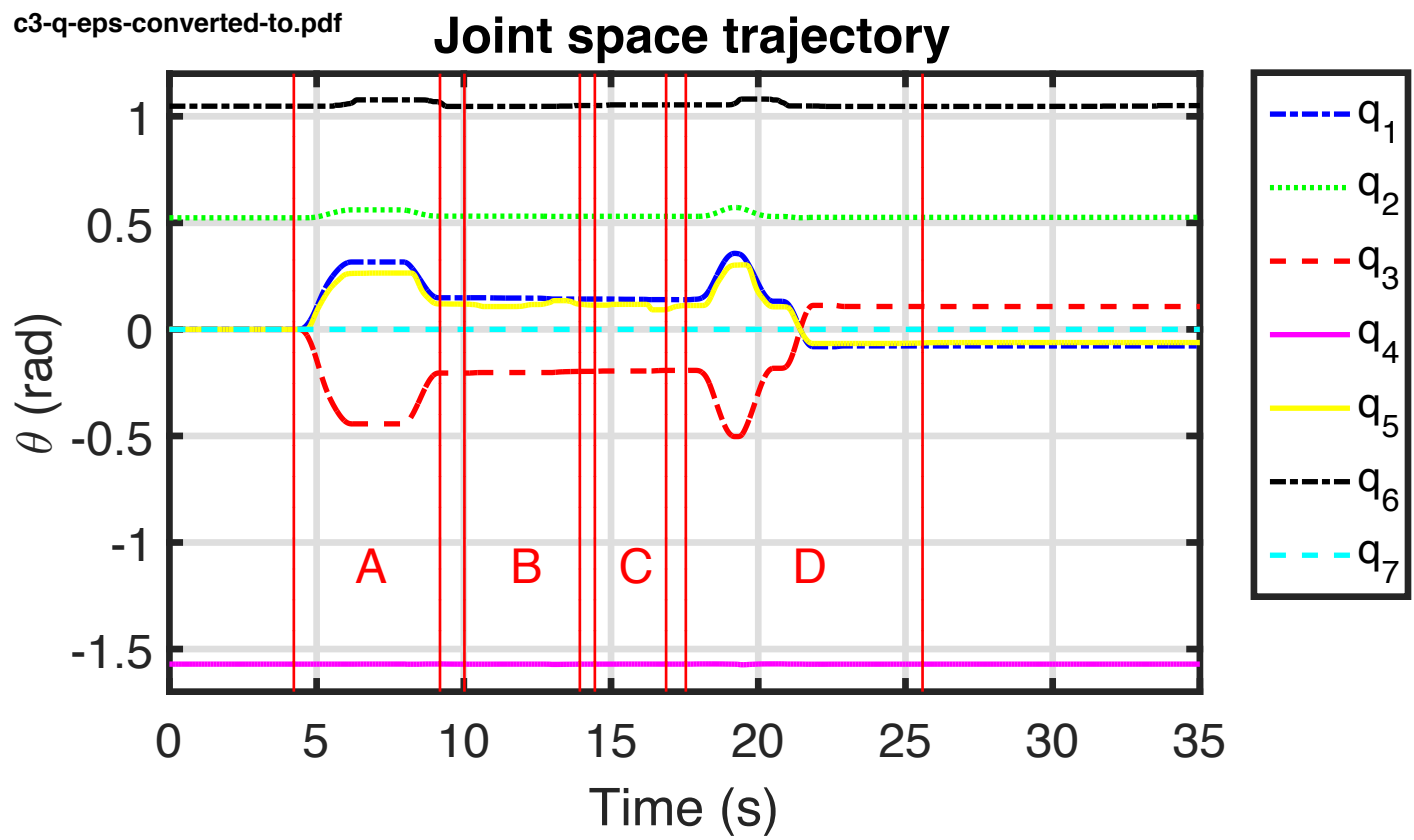
c3-q-eps-converted-to.pdf
Joint space trajectory
θ (rad)
Time (s)
A
B
C
D
q1
q2
q3
q4
q5
q6
q7

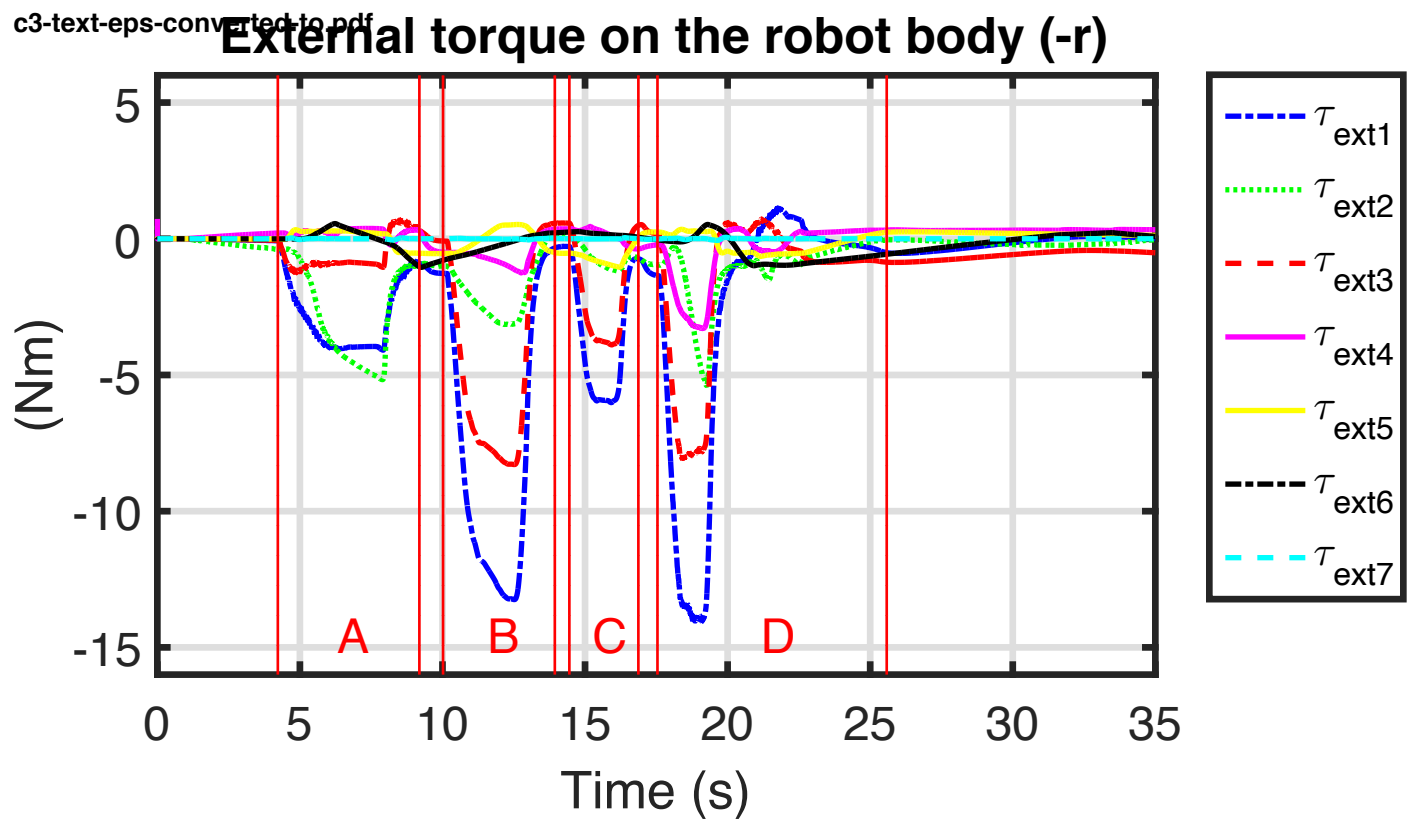

diag_rev2.png

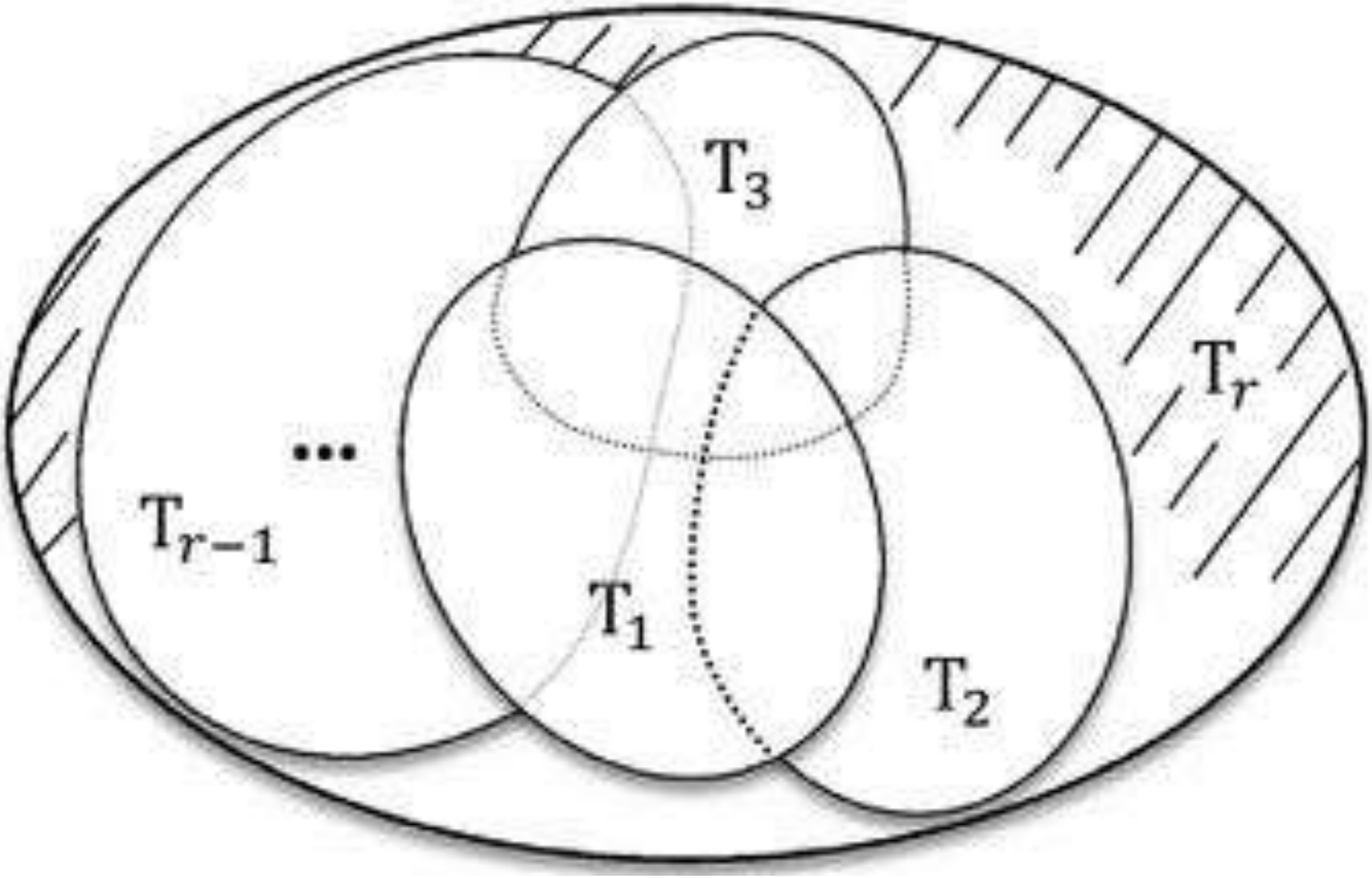

diag_state.png

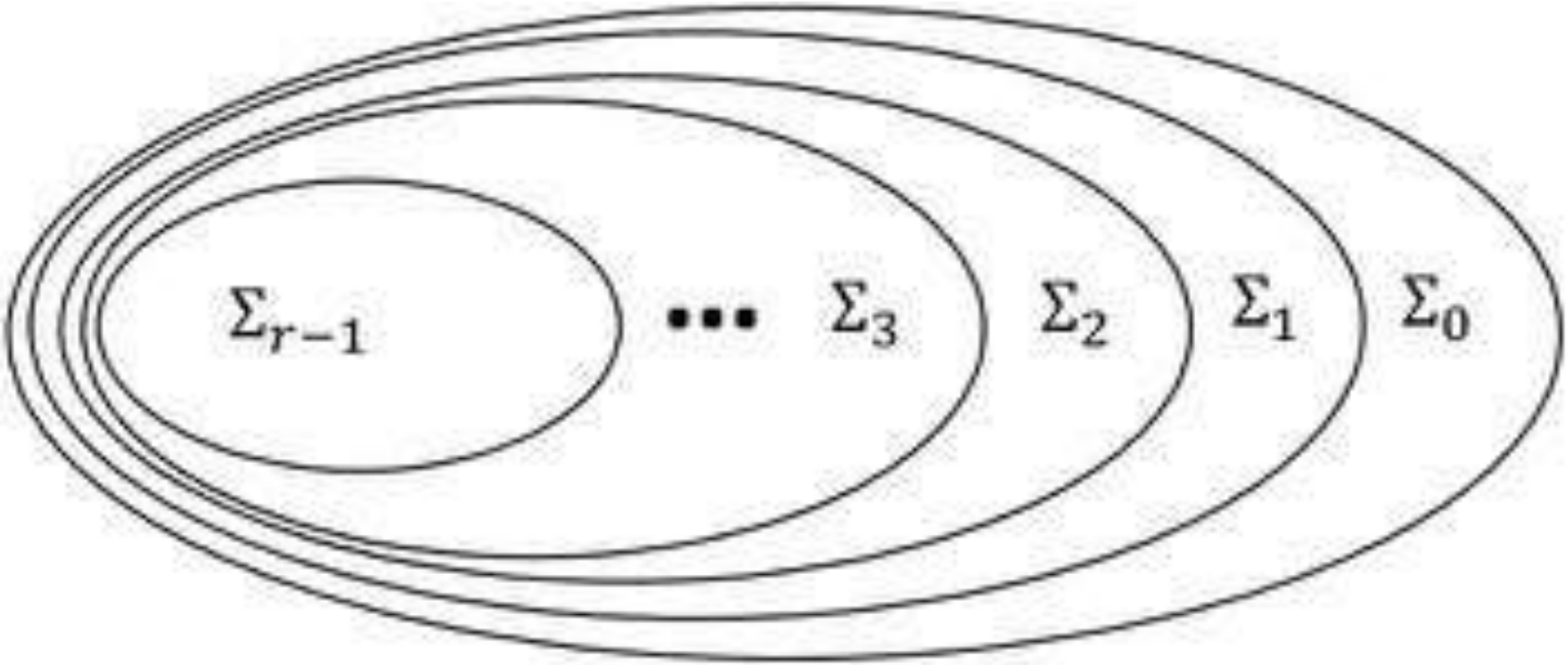

orientation.jpg

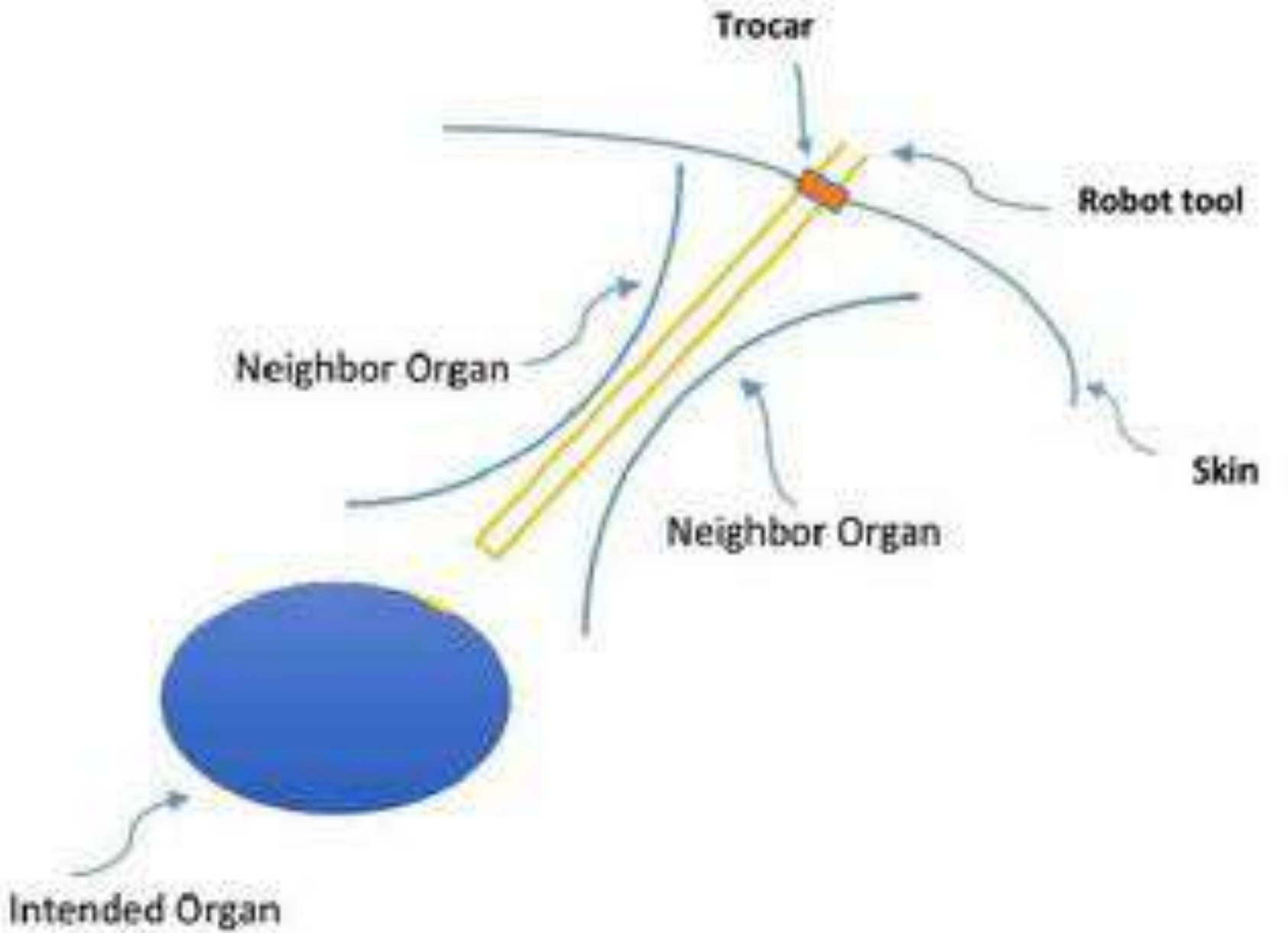

CONTROL ENGINEERING PRACTICE
Reply to Reviewers
Ms Number: CONENGPRAC-D-17-00852

Abbas Karami, Hamid Sadeghian, Mehdi Keshmiri, Giuseppe Oriolo

August 25, 2018

Type of submission: Regular Paper
Paper title: Force, Orientation and Position Control in Redundant Manipulators in Prioritized Scheme with Null-space Compliance

We respectfully thank the Associate Editor and the Reviewers for accurate reviewing of our work, Ms Number: D-18-00494, as well as for useful and valuable comments. We have revised our manuscript according to the reviewers' suggestions. In the following, both the original comments (*italic fonts*) and our replies (normal fonts) are reported. All the reference and equation numbers in our replies are given based on the revised manuscript reference numbering.

1 Reviewer #1; New Comments

I am not satisfied with the authors' answers A1-2 and A1-4 to my comments/suggestions R1-2 and R1-4, respectively.

- *Regarding A1-2: A nomenclature is indeed required to improve the readability of the manuscript.*

- *Regarding A1-4: The authors recommended (1) and (2) in the response document to be utilized to calculate (21). If it is the case then (1) and (2) should be given in the manuscript instead of (21) and then*

the new (22) should be found and further consequences in the stability analysis should also be investigated.

Answer:

First of all, we appreciate the respected reviewer regarding his concerns on our paper in order to improve this work.

- In the new revised manuscript, and based on the journal template, we have included a nomenclature in Section 2 (Table 1) to improve the readability and clearness of the paper.

- As mentioned in the paper, the momentum observer idea is originally proposed by A. De Luca et al. in [8] and further was extended in

  `Alessandro De Luca, Alin Albu-Schaffer, Sami Haddadin and Gerd HirzingerCollision, "Detection and Safe Reaction with the DLR-III Lightweight Manipulator Arm," IROS08,2008.`

  and some other papers afterwards. Recently, in

  `Emanuele Magrini Fabrizio Flacco Alessandro De Luca, "Control of Generalized Contact Motion and Force in Physical Human-Robot Interaction," ICRA015, 2015.`

  they use the residual vector $\boldsymbol{r}$ to localize the contact point during external interaction. A great survey in ths issue can be found in

  `S Haddadin, A De Luca, A Albu-Schffer, Robot collisions: A survey on detection, isolation, and identification," IEEE Transactions on Robotics 33 (6), 1292-1312, 2017.`

  As noted by the respected reviewer, the main concept is to **define** the vector $\boldsymbol{r}$ as

  $$\boldsymbol{r}(t) = \boldsymbol{K}_{obs}[\boldsymbol{p}(t) - \int_0^t (\boldsymbol{\tau} + \boldsymbol{C}^T\dot{\boldsymbol{q}} - \boldsymbol{g} - \boldsymbol{J}_f^T\boldsymbol{f}_f + \boldsymbol{r}(\sigma))d\sigma], \quad (21)$$

  such that the dynamics (22) is achieved. By this definition, the value $\boldsymbol{r}(t)$ is related the sum of its past values until the time $(t - \Delta(t))$, $\Delta(t) \to 0$, (and not the time t, itself) by the definition of the integral.

  Other quantities such as $\boldsymbol{M}(\boldsymbol{q})$, $\boldsymbol{C}(\boldsymbol{q}, \dot{\boldsymbol{q}})$, $\boldsymbol{g}(\boldsymbol{q})$ and $\boldsymbol{J}(\boldsymbol{q})$ can be obtained by the measured signal $\boldsymbol{q}$, $\dot{\boldsymbol{q}}$.

  By time derivation of (21) we have

  $$\dot{\boldsymbol{r}}(t) = \boldsymbol{K}_{obs}[\dot{\boldsymbol{p}}(t) - (\boldsymbol{\tau} + \boldsymbol{C}^T\dot{\boldsymbol{q}} - \boldsymbol{g} - \boldsymbol{J}_f^T\boldsymbol{f}_f + \boldsymbol{r}(t))].$$

Substituting the dynamics (1) and considering $\dot{\boldsymbol{p}} = \boldsymbol{M}\ddot{\boldsymbol{q}} + \dot{\boldsymbol{M}}\dot{\boldsymbol{q}}$, $\dot{\boldsymbol{M}} = \boldsymbol{C}+\boldsymbol{C}^T$, we reach to the dynamics (22) which gives a first order filtered version of external torque in Laplace form,

$$\frac{r_i(s)}{\tau_i(s)} = \frac{-K_{obs}}{s + K_{obs}} \tag{I}$$

The above dynamics is a continues dynamics and all the stability analysis are given for a continuous system. However, as we know, the controller is usually implemented on real system with high sampling rate, for instance $1ms$. Any method of integration can be used for $\boldsymbol{r}(t)$. To make the point more clear, the steps we followed in our C++ routine are shown in the following algorithm with Euler integration.

Algorithm 1 Calculation of $\boldsymbol{r}(t)$ at $t = t_1$ with sampling rate Δt

Input: initial values at $t = 0$,
$\boldsymbol{r}(0) = 0$, $\boldsymbol{p}(0) = 0$,
Integral=$\mathbf{0}$, $\Delta t = 0.001s$

Output: Find $\boldsymbol{r}(t_1)$

while $(t < t_1)$ **do**
  measure $\boldsymbol{q}$ **and** $\dot{\boldsymbol{q}}$ **from the encoders (at** $t = 0$, $\boldsymbol{q}(0) = \boldsymbol{q}_i$, $\dot{\boldsymbol{q}}(0) = 0$**)**
  calculate $\boldsymbol{M}(\boldsymbol{q})$, $\boldsymbol{g}(\boldsymbol{q})$, $\boldsymbol{C}(\boldsymbol{q})$, $\boldsymbol{J}(\boldsymbol{q})$, $\boldsymbol{f}_f$
  calculate the command torque $\boldsymbol{\tau}$**, by (19), (23-26)**
  Integral= Integral+$(\boldsymbol{\tau} + \boldsymbol{C}^T\dot{\boldsymbol{q}} - \boldsymbol{g} - \boldsymbol{J}_f^T\boldsymbol{f}_f + \boldsymbol{r}(t))\Delta t$
  calculate momentum $\boldsymbol{p}(t)$
  $\boldsymbol{r}(t)$**=**$\boldsymbol{K}_{0bs}$**(**$\boldsymbol{p}(t)$**-Integral)**
  apply command torque to the dynamics
  $t = t + \Delta t$
end while

Reviewer #1; Previous Comments

R1-2. *In its current form, the manuscript is hard to read and follow. The choice of mathematical notation may be one of the causes of this. A nomenclature may help improving the manuscript. Furthermore, time and/or state*

dependence of matrices and functions along with their dimensions should be given.

A1-2. All the formulations are checked by the authors and definition and dimension of all parameters are mentioned just after the first deceleration of parameter.

R1-4. *The definition of the residual vector in (21) is confusing (please notice that the authors used this in several of their past publications). Both the right and left hand sides of (21) has r(t) and it is not clear how to evaluate this accurately. It is clear to me that the authors introduced this to obtain (22). But the value of r at time "t" depends on its past values along with its value at time "t". Furthermore, the residual vector also required accurate knowledge of robot dynamics. In view of my above comments, the proposed strategy will work when robot dynamics is known and available accurately and when there is a mismatch then it will fail.*

A1-4.

As stated in the first paragraph of section 4 in the manuscript, the momentum observer idea is originally proposed by A. De Luca *et al.* in [8] (Eq. (5)) and later was exploited in [36]. This method is revised here to eliminate intentional physical interaction from undesired interactions. Computing this integral is straightforward by common numerical integration approaches. By using "trapezoidal method" for integration one can realize:

$$\begin{aligned}&\int_{t-\delta t}^{t}(\boldsymbol{\tau}+\boldsymbol{C}^T\dot{\boldsymbol{q}}-\boldsymbol{g}-\boldsymbol{J}_f^T\boldsymbol{f}_f+\boldsymbol{r}(\sigma))d\sigma]=\\&((\boldsymbol{\tau}(t)+\boldsymbol{C}(t)^T\dot{\boldsymbol{q}}(t)-\boldsymbol{g}(t)-\boldsymbol{J}(t)_f^T\boldsymbol{f}_f(t)+\boldsymbol{r}(t))+\\&(\boldsymbol{\tau}(t-\delta t)+\boldsymbol{C}(t-\delta t)^T\dot{\boldsymbol{q}}(t-\delta t)-\boldsymbol{g}(t-\delta t)-\boldsymbol{J}_f^T(t-\delta t)\boldsymbol{f}_f(t-\delta t)\\&+\boldsymbol{r}(t-\delta t)))\delta t/2.\end{aligned}\tag{II}$$

This equation can be replaced in (21)

$$\begin{aligned}&\boldsymbol{r}(t)=\boldsymbol{K}_{obs}(\boldsymbol{M}\dot{\boldsymbol{q}}-((\boldsymbol{\tau}(t)+\boldsymbol{C}(t)^T\dot{\boldsymbol{q}}(t)-\boldsymbol{g}(t)-\boldsymbol{J}(t)_f^T\boldsymbol{f}_f(t))+\\&(\boldsymbol{\tau}(t-\delta t)+\boldsymbol{C}(t-\delta t)^T\dot{\boldsymbol{q}}(t-\delta t)-\boldsymbol{g}(t-\delta t)-\boldsymbol{J}_f^T(t-\delta t)\boldsymbol{f}_f(t-\delta t)\\&+\boldsymbol{r}(t-\delta t)))\delta t/2)(1+\boldsymbol{K}_{obs}\delta t).\end{aligned}\tag{III}$$

and then $r(t)$ can be computed by using available data.

Supplementary Material for on-line publication only

Click here to download Supplementary Material for on-line publication only: Video.mp4

LaTeX Source Files

Click here to download LaTeX Source Files: main.zip